Taste quality interactions and transformations in a sensorimotor circuit

Philip K. Shiu *[,1], Gabriella R. Sterne *[,1, 2,^], Stefanie Engert[1], Barry J. Dickson[2, 3], and Kristin Scott[1,^,#]

[1] University of California, Berkeley, United States;

[2] Janelia Research Campus, Howard Hughes Medical Institute, United States;

[3] Queensland Brain Institute, University of Queensland, St Lucia, Queensland, Australia

* Equal first authors

^Corresponding authors: sternegr@berkeley.edu, kscott@berkeley.edu

[#] Lead contact

Summary

Taste detection and hunger state dynamically regulate the decision to initiate feeding. To study how context-appropriate feeding decisions are generated, we combined synaptic resolution circuit reconstruction with targeted genetic access to specific neurons to elucidate a gustatory sensorimotor circuit for feeding initiation in *Drosophila melanogaster*. This circuit connects gustatory sensory neurons to proboscis motor neurons through three intermediate layers. Most of the neurons in this pathway are necessary and sufficient for proboscis extension, a feeding initiation behavior, and respond selectively to sugar taste detection. Hunger signals act at select second-order neurons to increase feeding initiation in food-deprived animals. In contrast, a bitter taste pathway inhibits premotor neurons, illuminating a central mechanism that weighs sugar and bitter tastes to promote or inhibit feeding. Together, these studies reveal the neural circuit basis for the integration of external taste detection and internal nutritive state to flexibly execute a critical feeding decision.

Introduction

Feeding initiation is tightly regulated by food quality and internal nutritive state. Food quality is primarily evaluated by the gustatory system, which reports detection of both nutritious and noxious compounds in the environment. Food quality information must be integrated with internal nutritive state signals of hunger, satiety, or thirst to ensure that food intake matches energy demands. How do central neural circuits evaluate taste information in the context of internal nutritive state to make feeding decisions?

As feeding decisions are universal and essential for survival, diverse animals share similar strategies to detect taste compounds in the environment and assess nutrient needs. Peripheral taste detection in mammals and insects is mediated by sensory cells that detect specific taste modalities and elicit innate taste behaviors. Both mammals and flies have sugar-, bitter-, water-, and salt- sensing gustatory cells (Liman, et al., 2014; Yarmolinsky et al., 2009). Activation of sugar-sensing gustatory cells triggers feeding initiation, whereas activation of bitter-sensing gustatory cells inhibits feeding. Mammals and insects also evaluate internal nutrient needs with similar strategies (Augustine et al., 2018; Leopold and Perrimon, 2007; Pool and Scott, 2015; Nassel and Zandawala, 2019). Neuromodulators released from neurosecretory centers and the gut signal hunger or satiety to oppositely regulate feeding. Disruption of these hunger and satiety signals results in obesity and anorexia in mammals and insects.

To examine how the nervous system integrates external taste information and internal nutritive state to influence feeding, we turned to the *Drosophila melanogaster* model system, which offers the opportunity to interrogate how the brain computes

feeding decisions with synaptic resolution. Taste detection in insects begins with activation of gustatory receptor neurons (GRNs) found in sensory structures located on the body surface, including the external mouthparts, or proboscis labellum (Dethier, 1976; Stocker, 1994; Montell, 2021; Scott, 2018). From the periphery, the axons of proboscis GRNs project directly to the primary taste and premotor center of the insect brain, the subesophageal zone (SEZ) (Stocker and Schorderet, 1981; Kendroud et al., 2018; Miyazaki and Ito, 2010). The motor neurons that execute feeding have cell bodies and dendrites in the SEZ near GRN axons, suggesting a local feeding circuit (Gordon and Scott, 2009; McKellar et al., 2020; Schwarz et al., 2018). However, only a few isolated interneurons have been implicated in feeding initiation (Flood et al., 2013; Kain and Dahanukar, 2015).

To investigate how neural circuits transform taste detection into context-appropriate feeding decisions, we combined electron microscopy-based circuit reconstruction, genetic tools that provide access to single cell types, optogenetics, and imaging of taste responses in awake, behaving animals to uncover a circuit-level view of feeding initiation in *Drosophila melanogaste*r. This circuit is organized into an interconnected second-order neuron layer that synapses onto third-order and premotor layers. Most neurons are selectively activated by sugar taste detection and elicit feeding initiation behavior. Distinct circuit motifs allow flies to weigh food quality against hunger state to decide whether to initiate feeding. Hunger information acts on two second-order neurons, increasing pathway activity to promote the probability of initiating feeding upon food deprivation. Sugar and bitter tastes are weighed at premotor neurons, revealing a central mechanism that governs the decision between food acceptance or avoidance.

Together, this work delineates the neural circuit that transforms taste detection into the motor actions of feeding initiation and reveals how a central neural circuit integrates taste detection with internal physiological state to shape behavior.

Results

Gustatory receptor neurons synapse onto multiple second-order neurons

To examine neural circuits for feeding initiation, we began by identifying neurons directly postsynaptic to gustatory sensory axons in the central brain. We utilized the full adult fly brain (FAFB) electron microscopy (EM) volume (Zheng et al., 2018) to manually reconstruct neurons postsynaptic to 17 labellar GRN axons that likely correspond to sugar-sensing GRNs (Figures S1A and S1B) (Engert et al., 2021). Fifteen second-order taste neurons and their synapses were fully reconstructed (Figures 1A-1C and S1B-D) in the CATMAID platform (Saalfeld et al., 2009). The manually reconstructed neurons were compared with those in the recently released Flywire dataset, a dense, machine learning based reconstruction of FAFB neurons (Eckstein et al., 2020; Dorkenwald et al., 2020), revealing that they represent 12 of the 13 cell types with the most synapses from candidate sugar GRNs (Figure S1C; Table S1). These second-order neurons have not previously been characterized, except for G2N-1, which was identified as a candidate second-order gustatory neuron based on anatomical proximity to sugar-sensing GRNs (Miyazaki et al., 2015). Each of the second-order neurons is a local SEZ interneuron with arbors that overlap extensively with sugar GRN termini (Figures 1C and S1B).

Multiple second-order taste neurons influence proboscis extension

To test whether second-order gustatory neurons participate in feeding behaviors, we identified split-Gal4 lines that provide specific genetic access to individual second-order cell types. We compared the morphology of second-order EM reconstructions with a library of split-Gal4 lines that provides cell-type specific access to SEZ neurons (Sterne et al., 2021), using NBLAST analyses (Costa et al., 2016). This provided matches for 7 second-order neurons with split-GAL4 lines: Clavicle, G2N-1, Rattle, Fudog, Usnea, FMIn and Phantom (Figure 1D). Additionally, we used a triple intersection approach to gain specific genetic access to an eighth second-order neuron, Cleaver (Figure S2A), and generated split-Gal4 lines for a ninth, Zorro (Figure 1D). We confirmed that the Cleaver and Zorro split-GAL4 lines label the EM reconstructed neurons using NBLAST comparisons. The split-Gal4 lines are exquisitely specific for each of the 9 second-order gustatory neurons, providing the opportunity to evaluate their function.

As activation of sugar-sensing GRNs on the proboscis labellum causes the fly to extend its proboscis to initiate feeding (Dethier, 1976), we tested whether activation of second-order taste neurons elicits this behavior. We expressed the red-shifted channelrhodopsin CsChrimson (Klapoetke et al., 2014) selectively in each second-order taste neuron, activated each with 635 nm light, and examined the proboscis extension response (PER). Remarkably, optogenetic activation of 7 of the 9 second-order taste neurons elicited proboscis extension (Figures 2A and 2B). Activation of Cleaver and Fudog failed to cause proboscis extension (Figure S2B). Thus, multiple second-order gustatory neurons are sufficient to elicit feeding initiation, demonstrating that they activate downstream motor programs.

Because activation of seven classes of second-order taste neurons evokes proboscis extension, we next tested whether inhibiting their activity influences this behavior. We expressed the anion channelrhodopsin GtACR1 (Mohammad et al., 2017) in each neuron for optogenetic hyperpolarization of the neurons with 532 nm light, and tested PER to proboscis sucrose presentation in food-deprived flies (Figure 2C). Inhibiting six of the seven second-order neurons, Zorro, Clavicle, G2N-1, Rattle, Usnea, and FMIn, reduced PER to 50 mM sucrose, albeit only one of two G2N-1 and FMIn split-Gal4 lines had statistically significant decreases. Hyperpolarization of Phantom did not influence the probability of PER. At a higher sucrose concentration (100 mM), Usnea and Rattle inhibition decreased proboscis extension (Figure S2C), but inhibition of other neurons did not. These studies argue that multiple second-order neurons contribute to normal feeding initiation behavior and suggest that the partial redundancy of these second-order neurons ensures robust feeding.

Second-order taste neurons activate a local SEZ circuit for feeding initiation

How does activation of a diverse set of second-order neurons lead to activation of motor neurons that drive proboscis extension? Proboscis motor neurons have cell bodies and dendritic arbors in the SEZ near the axons of sugar GRNs, suggesting local circuitry (Gordon and Scott, 2009; Schwarz et al., 2017; McKellar et al., 2020). To locate proboscis motor neurons in the FAFB EM volume, we examined large SEZ neurons that lack synaptic output. Using this strategy, we identified proboscis motor neuron 9 (MN9) which extends the proboscis by contracting the rostrum protractor muscle and is required for feeding initiation (Gordon and Scott; McKellar et al., 2020). To identify a

pathway from taste detection to proboscis extension, we reconstructed presynaptic partners of MN9 and postsynaptic partners of second-order taste neurons.

By tracing upstream of MN9, we identified three premotor neurons, named Roundup, Rounddown and Roundtree (Figure 3A). Using Flywire neural reconstructions and a collection of automated synapse annotations (Buhmann et al., 2019), we found that Roundup, Roundtree and Rounddown are the 3rd, 5th and 15th most strongly connected neurons to MN9, respectively, and represent approximately 13% of the synapses onto MN9 (836 synapses of 6132 total; Table S1). Roundup and Rounddown are directly postsynaptic to subsets of second-order taste neurons, with Roundup receiving 30 synapses from G2N-1, 13 from Zorro and 6 from FMIn, and Rounddown receiving 37 synapses from G2N-1.

To characterize additional pathways from second-order neurons to motor neurons, we identified neurons upstream of premotor neurons and downstream of second-order taste neurons in the EM volume (Figure 3A). We reconstructed three third-order neurons, Sternum, Bract1, and Bract2, which connect second-order taste neuron subsets to premotor neurons (Figures 3A and 3B); Sternum and Bract2 provide 123 and 48 synapses onto Roundup, respectively. We also identified a previously characterized neuron, the putative feeding command neuron, Fdg (Flood et al., 2013) (Figures 3A and 3B). We place Fdg as a third-order neuron as it receives 17 synapses from second-order neurons FMIn and Rattle, and provides 49 synapses onto Bract1 and Bract2. Fdg also receives 4 synapses from candidate sugar GRNs. The third-order neurons identified here represent a small subset based on comparisons to Flywire automated reconstructions (Table S1). Thus, we have identified a minimal pathway from

taste detection to proboscis extension, composed of interconnected second-order neurons, third-order neurons each receiving inputs from a subset of second-order neurons, and feedforward premotor neurons.

To investigate the function of deeper layers of this circuit, we identified split-Gal4 lines that selectively label Bract and Fdg third-order neurons and the Roundup premotor neuron (Sterne et al., 2021), using NBLAST comparisons of EM reconstructions with SEZ split-Gal4 neural morphologies (Figure 3C). The Bract split-GAL4 lines label either Bract1 or Bract2, two morphologically similar and reciprocally-connected neurons identified in the EM volume. Optogenetic activation of Bract, Fdg or Roundup with CsChrimson revealed that each cell type elicits robust proboscis extension (Figure 3D). However, inhibiting Bract, Fdg or Roundup with GtACR1 did not influence PER to 50 mM sucrose (Figure 3E), consistent with multiple pathways to proboscis motor neurons. Thus, by combining EM tracing studies with precise neural manipulations afforded by split-Gal4 lines, we have elucidated a neural circuit that promotes feeding initiation upon sugar taste detection.

Feeding initiation neurons respond to sugar taste detection

To examine how taste information is processed by the feeding initiation circuit to guide feeding decisions, we monitored the activity of each of the neurons in the circuit to gustatory detection of water, sugar, or bitter taste solutions. The proboscis of live flies was stimulated with different taste solutions while imaging calcium changes in single SEZ neurons (Harris et al., 2015), using the GCaMP6s calcium indicator (Chen et al., 2013). These experiments revealed that most neurons in the feeding initiation circuit responded to sugar taste presentation in food-deprived animals (Figure 4). Five of the

seven second-order neurons responded only to presentation of sugar, and not to water or bitter solutions. Two second-order cell types responded to water stimulation: Usnea responded specifically to water taste detection and Phantom responded equally to water and sugar detection. Usnea and Phantom are reciprocally connected with GRNs (Table S1), suggesting that these second-order cell types may tune GRN responses in the presence of water. Fdg did not respond to proboscis taste stimulation, but did respond to optogenetic activation of sugar-sensing GRNs (Figure S3A). Third-order Bract and premotor neuron Roundup responded selectively to sugar taste presentation (Figure 4). Together, these studies reveal that sugar taste detection activates a multi-layered neural circuit to initiate feeding in hungry flies.

To test whether responses in the proboscis extension circuit are altered based on specific nutrient need, we examined taste responses in flies that were thirsty rather than hungry. High hemolymph osmolality is a key signal of thirst that acts on central neurons to promote water consumption (Jourjine et al., 2016). We bathed the brain in high osmolality artificial hemolymph to mimic a thirst-like state, which enhanced water responses in water-sensing GRNs (Figure S3B). Under these conditions, the response profiles of four of the five tested neural classes were identical to those observed in food-deprived flies (Figures 4 and S3C). However, one second-order neuron, Clavicle, changed its response profile in thirsty-like flies. Clavicle responded equally to water and to sugar tastants in a thirsty-like state but only to sugar in a hungry state (Figures 4 and S3C). These results suggest that the neurons uncovered here are largely dedicated to sugar taste detection regardless of whether the animal is hungry or thirsty. However,

state-dependent responses to water in thirsty flies at a single node (Clavicle) may tune the responsiveness of the pathway to bias acceptance of more dilute sugar solutions.

Feeding initiation is modulated by hunger at specific nodes

How is sugar taste information integrated with hunger state to promote feeding initiation in food-deprived flies? One site of hunger modulation is at the level of sugar GRNs (Inagaki et al., 2012; but see Kain and Danuhakar, 2015). However, whether sensory gating is the only mechanism for hunger regulation or whether modulation of central neurons contributes to an altered network state in hungry animals has not been examined. To comprehensively investigate how taste detection is integrated with hunger state to initiate feeding, we optogenetically activated each neuron in the PER circuit in either fed or food-deprived flies and examined behavior. Optogenetic activation has the advantage of bypassing changes in sugar sensory detection that propagate through the circuit, enabling the evaluation of central circuit changes.

We reasoned that activating neurons upstream, or at the node(s) where hunger modulation occurs, will cause differences in proboscis extension rates between hungry and fed flies. In contrast, activating neurons beyond the site where hunger impinges will result in no difference in proboscis extension rates between fed and starved flies. Indeed, CsChrimson-mediated activation of primary sugar-sensing neurons caused higher proboscis extension rates in food-deprived flies compared to fed flies, whereas activation of MN9 elicited the same proboscis extension rate in food-deprived and fed flies (Figures 5A-5C). A range of light intensities was used for optogenetic activation to mitigate differences in CsChrimson expression levels and to minimize ceiling effects (Figure 5B) (Chiu et al., 2021), and results were consistent across light intensities.

Thus, hunger modulation must occur at or beyond primary sugar-sensing neurons but before MN9.

We next optogenetically activated second-order, third-order and premotor neurons and measured proboscis extension in both food-deprived and fed flies. We found that activation of two second-order neurons, G2N-1 and Clavicle, increased proboscis extension in food-deprived flies as compared to fed flies, whereas activation of all other neural classes elicited the same response in food-deprived and fed flies (Figures 5A and 5D). Thus, we demonstrate that hunger signals act on a specific set of second-order interneurons in addition to sensory neurons (Inagaki et al., 2012). Third-order, premotor and motor neurons are not hunger-modulated. Modulation at specific second-order neurons provides an additional mechanism to amplify pathway activation and promote feeding initiation upon sugar taste detection in hungry animals.

Premotor neurons integrate sweet and bitter taste information

Animals evaluate both internal nutrient state and food quality to decide whether to initiate feeding. To investigate how food quality alters feeding initiation, we examined how the detection of bitter compounds is integrated with sugar taste information in the feeding initiation circuit. Previous studies have demonstrated that bitter compounds inhibit sugar-sensing gustatory neurons to prevent feeding (Chu et al., 2014; French et al., 2015; Jeong et al., 2013; Meunier et al., 2003). To investigate central mechanisms of bitter modulation, we examined whether pathways from bitter GRNs intersect with the feeding initiation pathway.

As bitter GRNs do not directly synapse with neurons in the feeding initiation circuit (Table S1), we asked whether second-order bitter neurons synapse onto the

feeding initiation pathway. We reconstructed second-order bitter taste neurons in the EM volume and identified a second-order bitter neuron we name Scapula, which receives over 150 synapses from bitter GRNs and is the second-most strongly connected cell type with bitter GRNs (Figure 6A, Table S1). Scapula synapses directly onto two feeding initiation premotor neurons, Roundup and Rounddown, but not onto second-order appetitive taste neurons.

Because bitter taste detection inhibits proboscis extension, we hypothesized that Roundup and Rounddown would be inhibited by Scapula to prevent proboscis extension to sugar in the presence of bitter compounds. To test this, we monitored activity in Roundup by *in vivo* calcium imaging while activating sugar GRNs, bitter GRNs, or both, using optogenetics to bypass sensory modulation. Roundup responded to optogenetic activation of sugar GRNs but not bitter GRNs (Figure 6B), as expected based on its response to taste solutions (Figure 4B). Upon co-activation of sugar and bitter GRNs, the Roundup response was dramatically decreased compared to the response to sugar GRN activation alone, arguing that bitter signals suppress the feeding initiation pathway. To test whether this bitter suppression reflects a central mechanism acting at Roundup, we monitored activity in a second-order neuron, G2N-1, directly upstream of Roundup, and found that its response upon co-activation of sugar and bitter GRNs was indistinguishable from its response to sugar GRN activation alone (Figure 6C). Together, the EM and imaging studies demonstrate that sugar and bitter tastes are integrated at the level of feeding initiation premotor neurons, providing a central mechanism to reject sweet foods laced with bitter compounds.

Discussion

Here, we identify a complete sensorimotor path from sugar taste detection to feeding initiation. Each neuron in this pathway is able to elicit proboscis extension and almost all respond selectively to sugar taste detection. Critical nodes tune pathway activity, increasing or decreasing responses in a context-dependent manner. These studies illuminate how sugar and bitter taste detection are integrated with hunger state to regulate feeding decisions.

A local, interconnected network transforms sweet taste detection into behavior

Previous studies in *Drosophila* have identified gustatory neurons that sense different taste modalities, motor neurons that regulate proboscis extension, and three candidate interneurons that influence the behavior (Gordon and Scott, 2009; McKellar et al., 2020; Flood et al., 2013; Kain and Dahanukar, 2015; Miyazaki et al., 2015; Talay et al., 2017). Here, by uncovering a complete sensorimotor circuit with synaptic resolution, we reveal a comprehensive view of the neural pathway that elicits proboscis extension, the first step in feeding. The feeding initiation pathway is a local circuit, with three- and four- synaptic relays to motor output. The six second-order, three third-order, one premotor, and one previously characterized motor neuron, MN9, all elicit proboscis extension upon optogenetic activation, showing the tight link of all relays to behavior. Interestingly, inhibiting activity of single second-order neurons reduced the behavioral response whereas inhibiting activity of third-order or premotor neurons did not. This partial redundancy of all nodes is consistent with the circuit architecture, revealing multiple paths from second-order neurons to premotor neurons. Connectivity analyses indicate that we have examined the function of most strongly connected second-order

sugar neurons but only a fraction of third-order and premotor neurons (Table S1). Thus, the pathway from second-order to motor neurons represents a minimal interconnected path, with sensory information becoming more distributed in deeper layers.

Most neurons in this pathway respond to sugar taste detection, but not water or bitter tastes, in food-deprived flies, demonstrating a direct line from sweet taste detection to motor output for feeding. How water taste modulates proboscis extension in thirsty flies will require further study. Importantly, we identified and characterized three second-order neurons that respond to water taste detection: one is selective for water taste, another responds to both water and sugar tastes, and a third shows state-dependent sugar and water taste responses. Further study of these second-order neurons and their connections will be critical to evaluate the degree of separation or convergence of water and sugar pathways for feeding initiation.

Of the interneurons identified here, only G2N-1 and Fdg have previously been implicated in feeding. G2N-1 was identified as a candidate sugar-sensing second-order neuron based on its anatomical proximity to gustatory axons alone (Miyazaki et al., 2015); here, we elucidated its role in taste detection and feeding initiation. Fdg was isolated as a “feeding command neuron”, able to elicit multiple steps in feeding, including proboscis extension (Flood et al., 2013). In our calcium imaging studies, Fdg did not respond to proboscis taste stimulation but did respond to optogenetic activation of sugar GRNs. This suggests that FDG may receive gustatory signals from GRNs on the pharynx or legs. Our studies demonstrate that Fdg is a third-order neuron in the feeding initiation pathway, with one synaptic relay to premotor neurons, well-poised to coordinate proboscis extension with other steps in feeding.

The architecture of the circuit provides a platform to investigate how taste signals are transformed in the brain to drive behavior. In this study, we focused on MN9, the rostrum protractor motor neuron that elicits proboscis extension, as a key readout of proboscis extension behavior. However, proboscis extension involves not only rostrum protraction but also extension of the haustellum and opening of the labellum, controlled by additional motor neurons (McKellar et al., 2020). We hypothesize that the connectivity among second-order and third-order neurons may coordinate the precise temporal activation of different muscle groups for coordinated extension. Moreover, proboscis extension is followed by ingestion then meal termination (Dethier, 1976; Pool and Scott, 2014). Continued expansion and exploration of this pathway will provide the opportunity to examine how different feeding subprograms are timed and coordinated to elicit feeding in natural environments.

Hunger tunes second-order neurons to promote sugar responses

Responses to taste compounds vary based on nutritional status. Studies in *C. elegans*, *Drosophila*, and mammals have demonstrated that a key site of regulation is at the peripheral chemosensory neurons, altering sensitivity of detection (Chalasani et al., 2010; Kawai et al., 2000; Root et al., 2011; Savigner et al., 2009; Sengupta, 2013). For example, dopamine modulates the sensitivity of *Drosophila* sugar-sensing gustatory neurons to promote proboscis extension at lower sucrose concentrations (Inagaki et al., 2012; Marella et al., 2012). Hunger modulation of taste processing beyond sensory neurons has been more challenging to evaluate, both because of lack of knowledge of central networks and because changes at the sensory level propagate through the network.

To isolate the role of central brain neurons in hunger modulation, we used the single-cell genetic precision available in *Drosophila* to activate each node of the feeding initiation pathway and examined the behavioral response elicited in fed and food-deprived flies. These studies pinpoint the site of hunger modulation to sensory neurons and two second-order neurons. Although caveats of artificial stimulation exist, the consistent changes seen across different light intensities for neural manipulation early in the pathway, but not downstream, argues that these results are robust. These studies demonstrate that hunger acts at a few critical nodes to modulate feeding initiation: sensory neurons increase detection sensitivity and second-order neurons amplify pathway activation. It will be interesting to examine whether hunger modulation of sensory and second-order neurons occurs independently or over different time scales to adjust behavioral responses as starvation increases. In addition, the specific hunger signals that act on central neurons and their mechanism of modulation may now be explored.

Bitter compounds inhibit premotor neurons to prevent feeding initiation

Recent studies have begun to investigate how sweet and bitter taste information is integrated in the brain to influence feeding decisions (Jin et al., 2021; Peng et al., 2015; Wang et al., 2018). In *Drosophila*, bitter taste compounds directly decrease sugar sensory activity, both by binding to proteins on sugar gustatory neurons and by presynaptic inhibition (Chu et al., 2014; French et al., 2015; Jeong et al., 2013; Meunier et al., 2003). To investigate whether there are also central pathways that integrate sugar and bitter taste detection, we examined neurons postsynaptic to bitter gustatory axons and identified second-order bitter neurons that directly synapse onto proboscis premotor

neurons for feeding initiation. Moreover, we show that bitter signals inhibit sugar responses in premotor neurons but not in upstream neurons. The convergence of bitter and sugar signals at the level of premotor neurons provides an elegant strategy to weigh incoming sugar and bitter taste information and adjust behavioral probability. In addition, by blocking activity at specific muscles, bitter detection may specifically change behavior to direct the proboscis away from a hazardous food source.

In mammals, a pathway from the bitter gustatory cortex provides feedback inhibition onto sugar-sensing brainstem circuits to prevent consumption of bitter-sweet mixtures (Jin et al., 2021). In addition to cortical feedback, we propose that local brainstem circuits may also directly integrate bitter and sweet signals and suppress licking motor programs, analogous to the local *Drosophila* circuit reported here.

In this study, we coupled EM circuit reconstruction with the ability to precisely monitor and manipulate single neurons to elucidate how a complex nervous system orchestrates the decision to initiate feeding. These studies demonstrate central modules that integrate taste detection with internal state, providing insight into how taste modalities and feeding decisions are encoded in the brain.

Acknowledgments

We thank Lori Horhor, Jolie Huang, Neil Ming, Vivian Nguyen, Andrea Sandoval, Neha Simha, Rivka Steinberg, and Parisa Vaziri for EM tracing contributions. Vivek Jayaraman provided unpublished fly lines used in this study. This work was supported by NIH R01DC013280 (K.S.), NIH F32DK117671 (G.R.S.) and NIH F32DC018225 (P.S.). Neuronal reconstruction for this project took place in a collaborative CATMAID environment in which 27 labs are participating to build connectomes for specific circuits. Development and administration of the FAFB tracing environment and analysis tools were funded in part by National Institutes of Health BRAIN Initiative grant 1RF1MH120679-01 to Davi Bock and Greg Jefferis, with software development effort and administrative support provided by Tom Kazimiers (Kazmos GmbH) and Eric Perlman (Yikes LLC). Peter Li, Viren Jain and colleagues at Google Research shared automatic segmentation (Li et al., 2019). We thank members of the Flywire community for their proofreading contributions. Confocal imaging for triple intersection characterization was conducted at the CRL Molecular Imaging Center, supported by the Helen Wills Neuroscience Institute and NSF DBI-1041078. We would also like to thank Holly Aaron and Feather Ives for their microscopy training and assistance. Members of the Scott lab provided comments on the manuscript.

Author Contributions

P.K.S. and G.R.S. conceived and performed experiments and analyzed the data under guidance from K.S. P.K.S. and S.E. performed EM analyses, P.K.S. and G.R.S. performed behavioral analyses, G.R.S. performed calcium imaging studies. G.R.S.,

B.J.D., and K.S. collaborated in the generation of split-Gal4 lines for these studies. P.K.S., G.R.S., and K.S. wrote the manuscript. B.J.D. and S.E. provided advice and guidance on the work.

Declaration of Interests

The authors declare no competing interests.

Figure 1

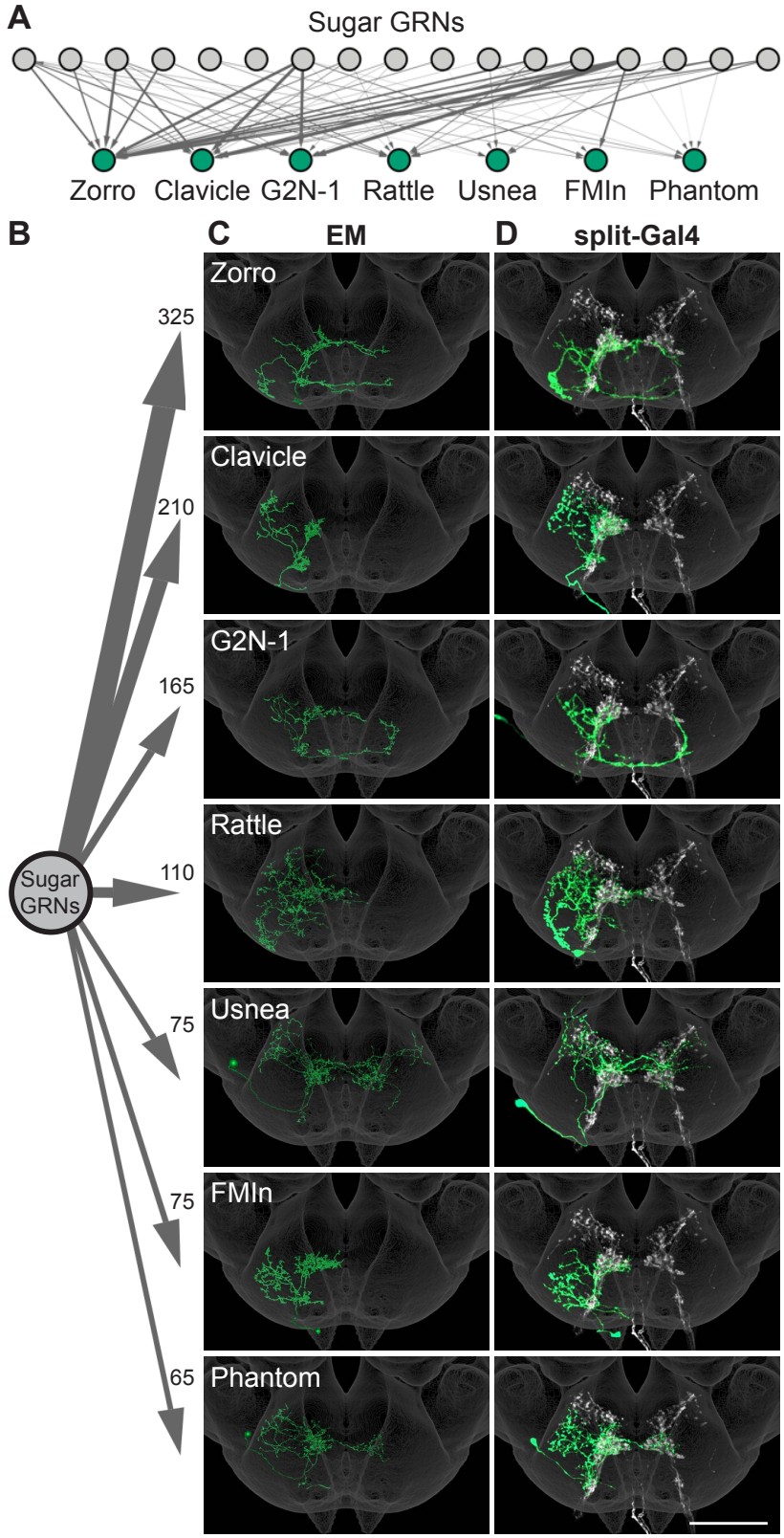
A
Sugar GRNs
Zorro
Clavicle
G2N-1
Rattle
Usnea
FMIn
Phantom
B
C
EM
D
split-Gal4
Sugar GRNs
325
210
165
110
75
75
65
Zorro
Clavicle
G2N-1
Rattle
Usnea
FMIn
Phantom

Figure 1. Sugar-sensing GRNs synapse onto multiple second-order neurons. (A) Synaptic connectivity of 17 previously identified candidate sugar GRNs onto second-order sugar neurons. Line thickness represents the number of synapses, with a minimum of 6 synapses to a maximum of 46 synapses. (B) Aggregate synaptic connectivity from sugar GRNs onto second-order sugar neurons. Numbers indicate the total number of synapses that the 17 candidate sugar GRNs make onto each second-order neuron. (C-D) Manually reconstructed EM skeletons (C) and registered neural images in split-Gal4 lines (D) for each second-order neuron in the subesophageal zone of the *Drosophila* brain. Sugar GRNs are depicted in white in (D). See also Figure S1 for EM reconstructions of additional second-order neurons and Table S1 for synaptic connectivity counts.

Figure 2

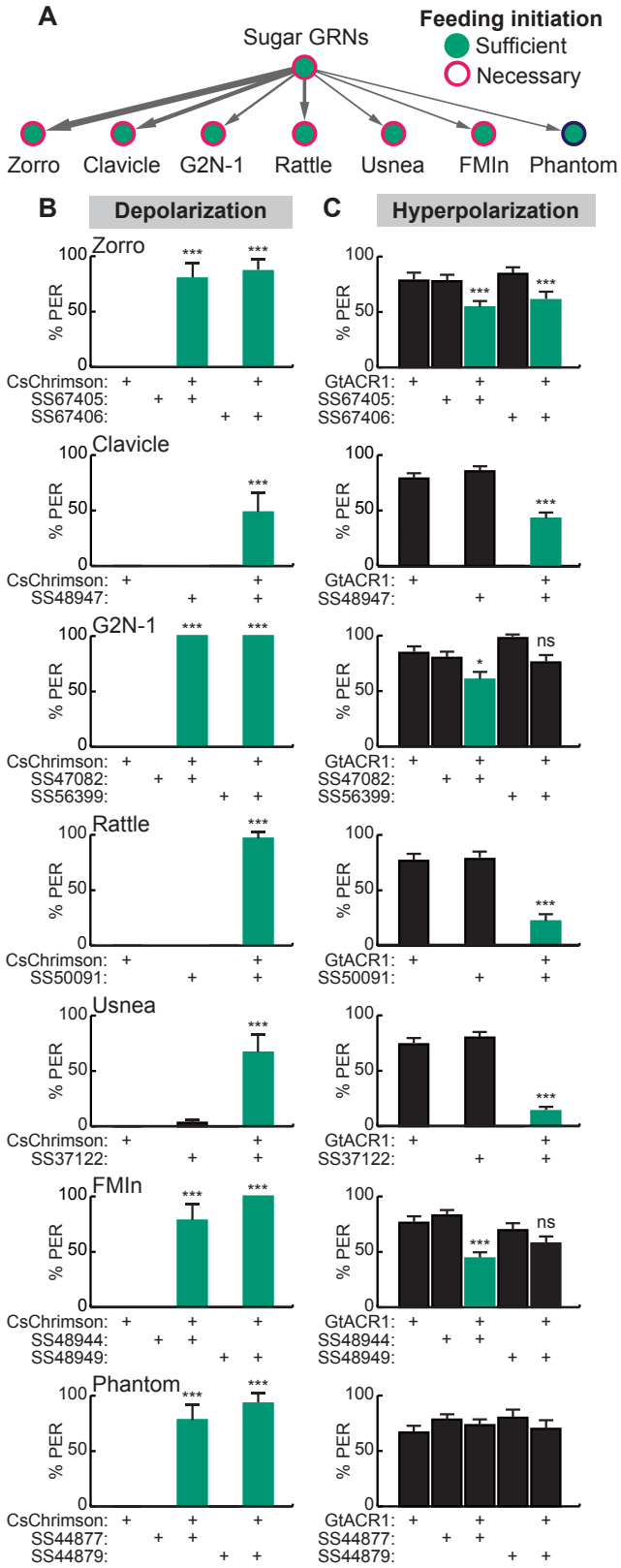
A
Sugar GRNs
Feeding initiation
Sufficient
Necessary
Zorro
Clavicle
G2N-1
Rattle
Usnea
FMIn
Phantom
B
Depolarization
C
Hyperpolarization
% PER
CsChrimson:
GtACR1:
SS67405:
SS67406:
SS48947:
SS47082:
SS56399:
SS50091:
SS37122:
SS48944:
SS48949:
SS44877:
SS44879:
ns

Figure 2. Activation and inhibition of second-order taste neurons influences proboscis extension. (A) Schematic of proboscis extension phenotypes of second-order neurons, line thickness corresponds with total synaptic connectivity. (B) CsChrimson-mediated activation of seven second-order neurons elicits proboscis extension. n=30 flies per genotype. (C) GtACR1-mediated inhibition of second-order neurons reduces proboscis extension to 50 mM sucrose. n= 46-83 flies per genotype. (B-C) Shown are the fraction of flies exhibiting PER upon optogenetic or 50 mM sucrose stimulation. Mean ± 95% confidence interval (CI), Fisher's Exact Tests, *$p<0.05$, ***$p<0.001$. See also Figure S2 for additional PER phenotypes of second-order sugar neurons.

Figure 3

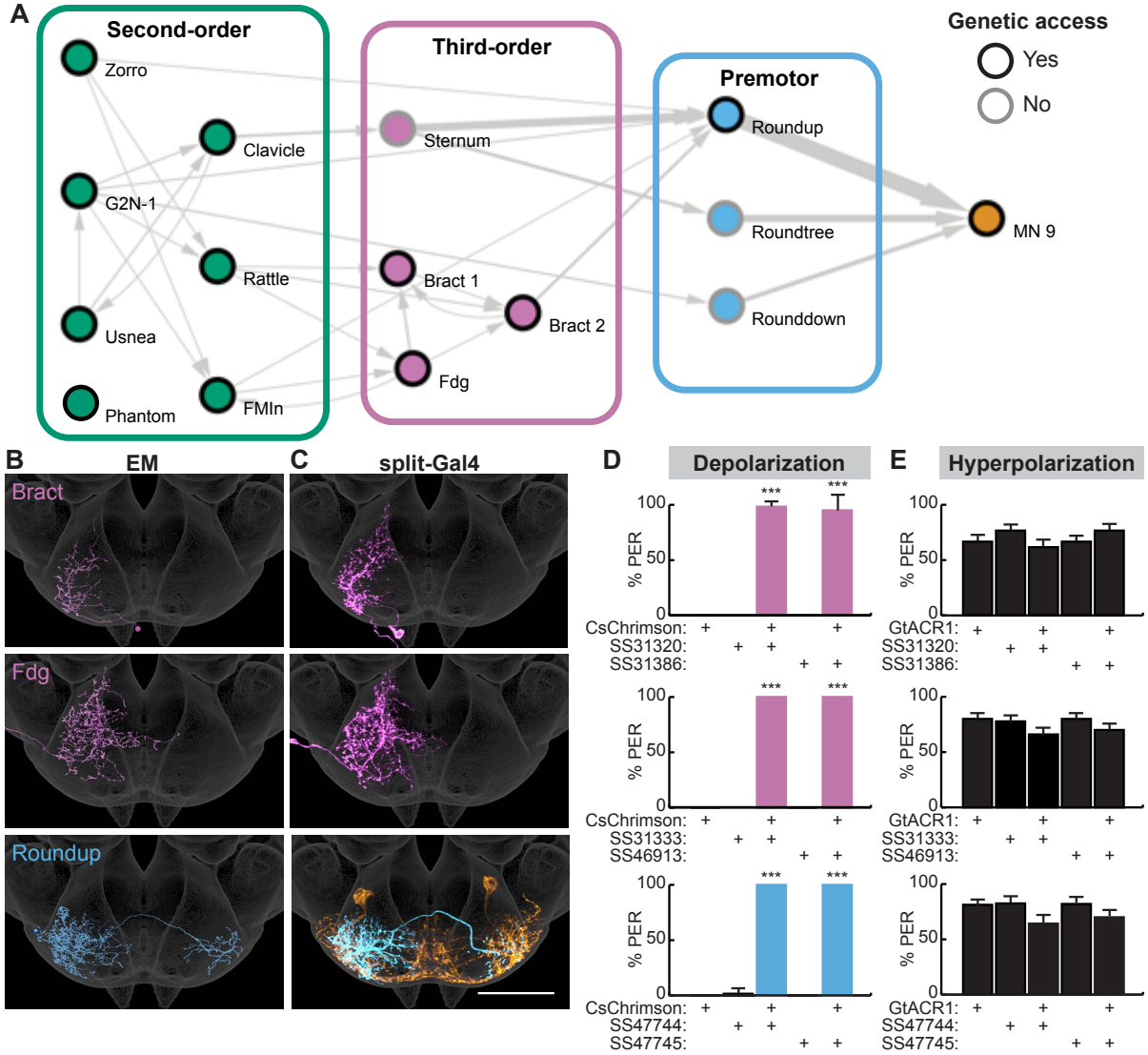

Figure 3. Second-order neurons synapse onto a local sensorimotor circuit for feeding initiation. (A) Schematic of the feeding initiation circuit. Black circles denote neurons with split-Gal4 genetic access, gray circles denote neurons without split-Gal4 genetic access. Line thickness represents synaptic connectivity of more than 5 synapses. (B-C) EM neural reconstructions (B) and registered neural images in split-

Gal4 lines (C) of third-order or premotor neurons in the SEZ. (D) Cs-Chrimson-mediated activation of third-order or premotor neurons elicits PER. n=30 flies per genotype. (E) GtACR1-mediated inhibition of third-order or premotor neurons does not influence PER to 50 mM sucrose. n=40-70 flies per genotype. (D-E) Mean ± 95% CI, Fisher's Exact Tests, ***$p<0.001$.

Figure 4

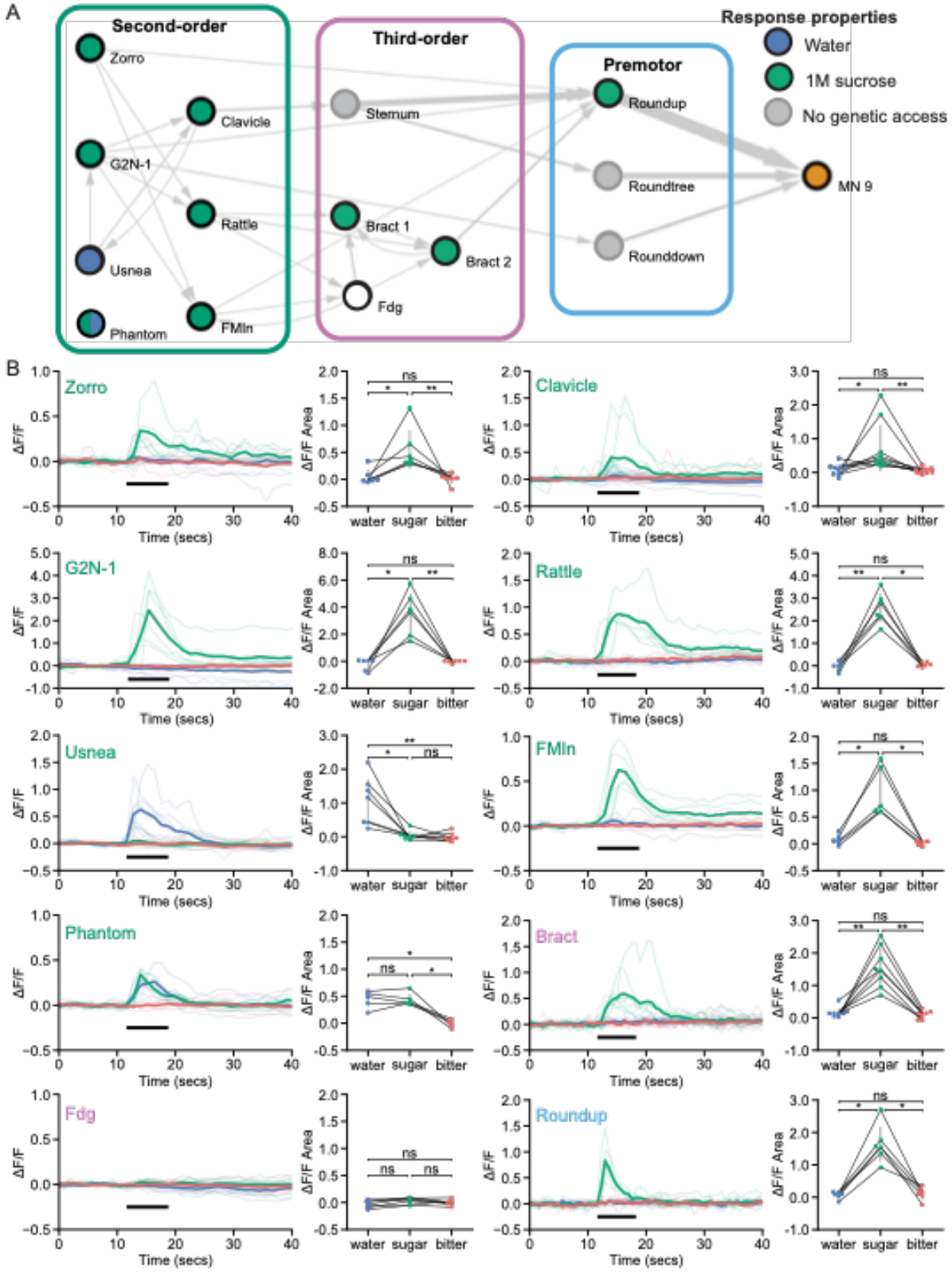
A
Second-order
Zorro
Clavicle
G2N-1
Rattle
Usnea
Phantom
FMIn
Third-order
Sternum
Bract 1
Bract 2
Fdg
Premotor
Roundup
Roundtree
Rounddown
MN 9
Response properties
Water
1M sucrose
No genetic access
B
Zorro
Clavicle
G2N-1
Rattle
Usnea
FMIn
Phantom
Bract
Fdg
Roundup
ΔF/F
ΔF/F Area
Time (secs)
water
sugar
bitter
ns

Figure 4. Feeding initiation neurons respond to taste detection. (A) Connectivity schematic of the feeding initiation circuit, where filled green circles represent cell types that respond to sugar detection, while filled blue circles represent cell types that respond to water detection. One cell type, Phantom, responds to both sugar and water (split blue and green circle). FDG did not respond to proboscis taste detection (white circle), but see Figure S4A for responses to optogenetic activation of sugar GRNs. (B) Calcium responses of feeding initiation neurons to stimulation of the proboscis in starved flies. For each cell type, GCaMP6s fluorescence traces are shown on the left of the panel (ΔF/F), while ΔF/F area for each trace is shown on the right, with thin black lines indicating sample pairing. The proboscis of each tested individual was stimulated with water (green), sugar (blue), and bitter (red) tastants in sequential trials during the indicated period (thick black line). The following split-GAL4 lines were imaged for each cell type: Clavicle; SS48947, FMIn; SS48944, Zorro; SS67405, G2N-1; SS47082, Usnea; SS37122, Phantom; SS68204, Rattle; SS50091, Fdg; SS31345, Bract; SS31386, Roundup; SS47744. Quade's Test with Quade's All Pairs Test, using Holm's correction to adjust for multiple comparisons, ns $p>0.05$, *$p\leq0.05$, **$p\leq0.01$. See also Figure S3 for additional calcium imaging studies of feeding initiation neurons.

Figure 5

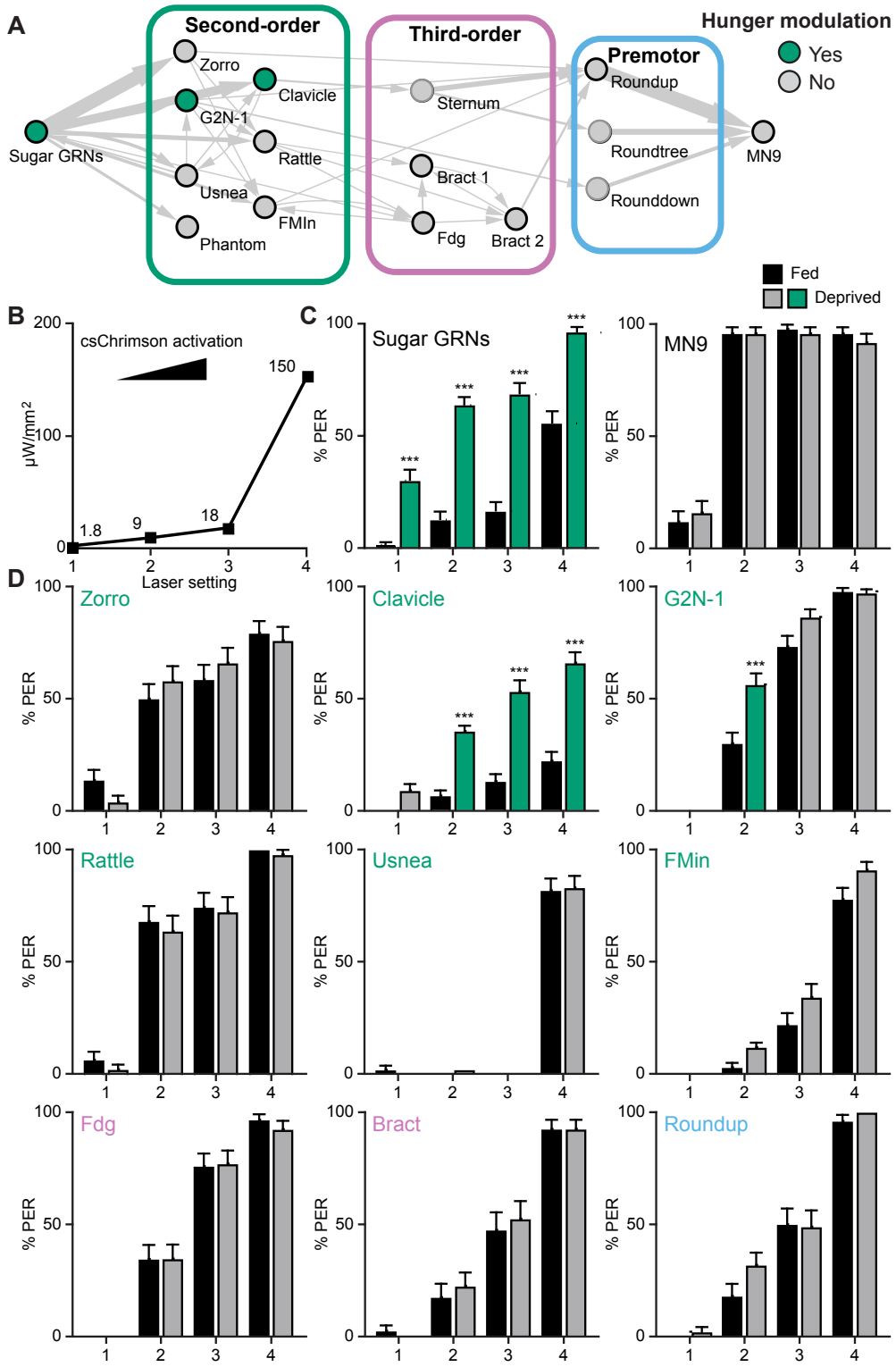
A
Second-order
Third-order
Premotor
Hunger modulation
Yes
No
Zorro
Clavicle
G2N-1
Rattle
Usnea
FMIn
Phantom
Sugar GRNs
Sternum
Bract 1
Fdg
Bract 2
Roundup
Roundtree
Rounddown
MN9
Fed
Deprived
B
csChrimson activation
µW/mm²
Laser setting
1.8
9
18
150
C
Sugar GRNs
MN9
% PER
D
Zorro
Clavicle
G2N-1
Rattle
Usnea
FMin
Fdg
Bract
Roundup

Figure 5. Hunger acts on a subset of second-order central neurons to modulate behavior. (A) Schematic of the feeding initiation circuit, with filled green circles representing nodes that are hunger-modulated. (B) Optogenetic activation at four different light intensities. (C) Activation of sugar-sensing neurons results in different feeding initiation rates between fed and food-deprived flies (left) whereas activation of MN9 does not (right), at four different light intensities. n=50. (D) Optogenetic activation of second-order, third-order, and premotor neurons in either fed or food-deprived flies. n= 39-103. Mean ± 95% CI, Fisher's Exact Tests, ***$p<0.001$

Figure 6

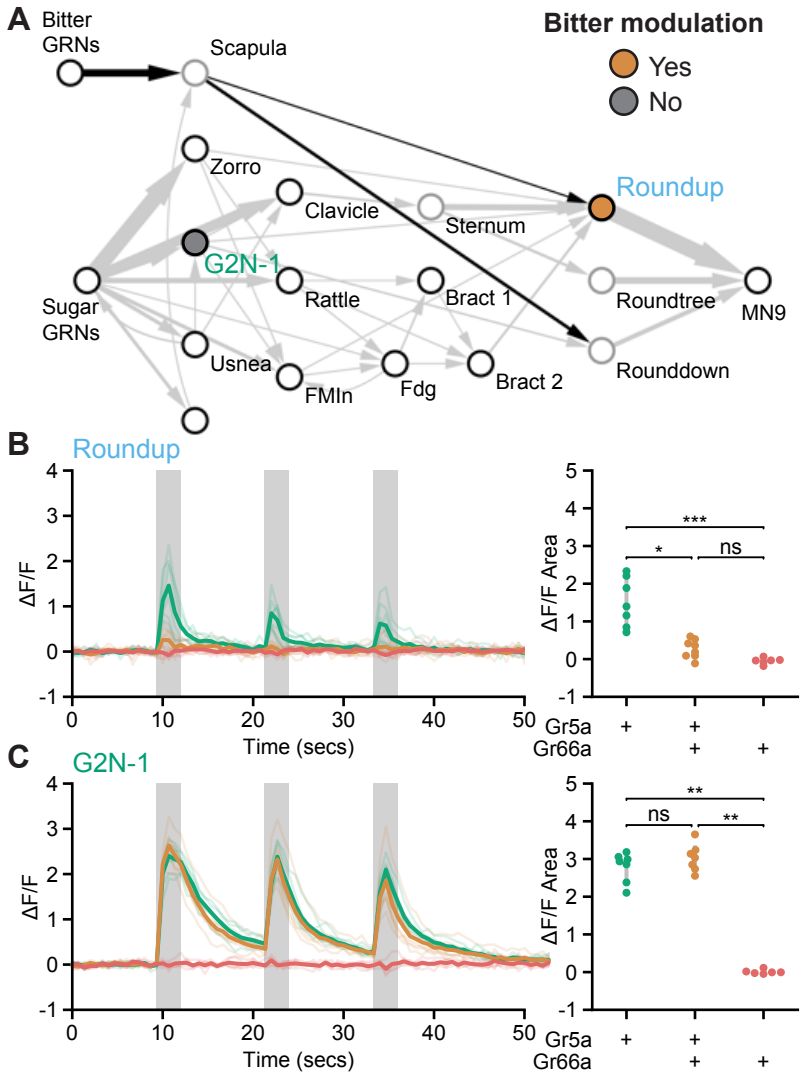

Figure 6. Premotor neurons integrate sweet and bitter taste detection. (A) Schematic of the feeding initiation circuit, showing a pathway from bitter GRNs to premotor neurons. Filled maize circle labels a premotor neuron inhibited by bitter tastants, filled grey circle labels an upstream second-order neuron that is not inhibited by bitter tastants. (B and C) Calcium responses of feeding circuit neurons to optogenetic activation of sugar (green, Gr5a-LexA), sugar plus bitter (maize, Gr5a-LexA plus Gr66a-LexA), or bitter (red, Gr66a-LexA) GRNs in starved flies. For each cell type,

Syt::GCaMP7b fluorescence traces are shown on the left of the panel (ΔF/F), while ΔF/F area for each trace is shown on the right. Periods of stimulation with 660 nm light are indicated with vertical grey bars. (B) SS47744 was imaged to examine Roundup responses. (C) SS47082 was imaged to examine G2N-1 responses. Kruskal Wallace test with Dunn's test using Holm's correction to adjust for multiple comparisons, ns $p>0.05$, *$p\leq0.05$, **$p\leq0.01$, ***$p\leq0.001$.

STAR METHODS

RESOURCE AVAILABILITY

Lead contact

Further information and requests for resources and reagents should be directed to and will be fulfilled by the Lead Contact, Kristin Scott (kscott@berkeley.edu).

Materials availability

This study did not generate new unique reagents. All fly lines will be available upon request.

Data and code availability

Data reported in this paper will be shared by the lead contact upon request.

EXPERIMENTAL MODEL AND SUBJECT DETAILS

Rearing conditions and strains

All experiments were performed in the fruit fly *Drosophila melanogaster*. The key resources table lists the transgenic lines used in this study. Flies were reared on standard cornmeal-yeast-molasses media at 25°C with 65% humidity and a 12hr: 12hr light: dark cycle unless stated otherwise. Flies for optogenetic experiments were raised on standard food in darkness. Upon eclosion, adult flies were collected and maintained on standard food supplemented with 0.4 mM all-trans-retinal in darkness prior to experiments. Adult mated female flies were used for all experiments.

METHOD DETAILS

Electron Microscopy Neural Reconstructions

Second-order neurons were reconstructed in a serial section transmission electron volume (Full Adult Female Brain, Zheng et al., 2018) using the CATMAID software (Saalfeld et al., 2009). Fully manual reconstructions were generated by following the branches of the neuron and marking the center of each branch, thereby creating a “skeleton” of each neuron. In addition to fully manual reconstructions, segments of an automated segmentation (Li et al., 2020) were proofread and expanded to generate complete reconstructions. To specifically reconstruct second-order sugar neurons, two different methods were used. First, random presynapses of skeleton 7349219 (Engert et al., 2021) were chosen using the reconstruction sampler function of CATMAID and downstream partners were reconstructed. Second, large automatically generated fragments downstream of sugar GRN axons were found, and expanded. Chemical synapses were annotated as previously described (Zheng et al., 2018); specifically, at least three of four elements of a synapse were needed to call a synapse: a T-bar, postsynaptic density, synaptic vesicles, and a synaptic cleft. All reconstructions for which there is a corresponding split-Gal4 were assembled and proofread to near completion.

Flywire connectivity analysis

Neurons corresponding to those traced in CATMAID were located in Flywire (Flywire.ai); both reconstructions use the same underlying EM data (Zheng et al., 2018). To identify neurons upstream or downstream of a set of Flywire neurons, we used CAVE (connectome annotation versioning engine; Buhmann et al., 2021; Heinrich et al., 2018). To identify synapses of fairly high confidence, we chose a "cleft_score" cutoff of 100 (Heinrich et al., 2018).

Genetic access to Cleaver

To gain specific genetic access to Cleaver, we used a triple intersection approach. In this approach, csChrimson-mVenus will only be expressed where the expression patterns of the AD, DBD, and LexA overlap. SS31022 (Sterne et al. 2021) labels both Cleaver and Usnea. To specifically access Cleaver, virgins of 20xUAS>dsFRT>csChrimson-mVenus;8XLexAop2-FLPL(attP40);Dfd-LexA were crossed to males of SS31022. To specifically access Usnea in SS31022, virgins of 20xUAS>dsFRT>csChrimson-mVenus;8XLexAop2-FLPL(attP40);Scr-LexA were crossed to males of SS31022. For each intersection, female progeny without balancers were selected for behavioral analysis.

To visualize triple intersection expression patterns, brains were dissected as described (https://www.janelia.org/project-team/flylight/protocols, 'Dissection and Fixation 1.2% PFA').

The following primary antibodies were used:

-1:40 mouse α-Brp (nc82) (DSHB, University of Iowa, USA)

-1:1000 chicken α-GFP (Invitrogen A10262)

The following secondary antibodies were used:

-1:500 α-mouse AF647 (Invitrogen, A21236)

-1:1000 α-chicken AF488 (Life Technologies, A11039)

Immunohistochemistry was carried out as described (https://www.janelia.org/project-team/flylight/protocols, 'IHC-Anti-GFP') substituting the above antibodies and eschewing the pre-embedding fixation steps. Ethanol dehydration and DPX mounting was carried out as described (https://www.janelia.org/project-team/flylight/protocols, 'DPX

Mounting'). Images were acquired with a Zeiss LSM 880 NLO AxioExaminer. A Plan-Apochromat 25×/0.8 objective was used at zoom 0.7. Acquired images had a voxel size of 0.59 µm × 0.59 µm × 1.50 µm.

NBLAST Analysis

NBLAST analysis was used to match neurons reconstructed in EM to neurons labeled by split-GAL4 lines (Costa et al., 2014). Reconstructed neurons from CATMAID were transformed into the JRC2018U template space using NAVIS (Bates et al., 2020; Schlegel, et al., 2021) and compared to a light-level library of 122 SEZ cell types in the SEZ split-GAL4 collection (Sterne et al., 2021). In addition, we added a representative image from a split-GAL4 we designed to cover a cell type reported here, Zorro, using previously described methods (Sterne et al., 2021). Each reconstructed neuron on the right of the brain was compared to every SEZ cell type in the library using the natverse toolkit in R (Bates et al., 2020). Normalized, mean scores were calculated to control for neuron size and segment number. The highest scoring light-level cell type for each reconstructed neuron was considered a match if the normalized, mean NBLAST score was greater than 0.4.

Reconstructed cell types with matches include the following *FAFB IDs* (Top match cell type, NBLAST score): *Bract1* (Bract, 0.58), *Bract2* (Bract, 0.57), *Clavicle* (Clavicle, 0.54), *Cleaver* (Cleaver, 0.57), *Fdg* (Fdg, 0.64), *FMIn* (FMIn, 0.61), *Fudog R* (Fudog, 0.43), *G2N-1* (G2N-1, 0.49), *Phantom* (Phantom, 0.67), *Rattle* (Rattle, 0.60), *Roundup* (0.63), *Usnea* (Usnea, 0.50), *Zorro R* (Zorro, 0.54).

Reconstructed cell types which did not return matches include the following *FAFB IDs* (Top match cell type, NBLAST score): *Billiards* (Phantom, 0.17), *Buster*

(Marge, 0.30), *Dandelion* (Clavicle, -0.16), *Fuchs* (Phantom, 0.37), *Quasimodo* (Puddle, 0.32), *Rounddown* (Roundup, 0.28), *Roundtree* (Puddle, 0.27), *Specter* (Usnea, 0.16), *Sternum* (Rattle, 0.10).

Optogenetic Activation

PER was scored as previously described (Mann, Gordon and Scott, 2013). Female flies were raised on standard cornmeal-yeast-molasses medium, until 48 hours before experiments, when flies were placed on molasses food with 0.4 mM retinal. Three to five-day-old flies were anesthetized with carbon dioxide, mounted onto a glass slide with nail polish, and allowed to recover for two hours in a humidified chamber at 22°C. For experiments in Figure 2A, flies were activated with 153 uW/mm^2 635 nm laser light (Laserglow). Flies were scored for whether they extended their proboscis within a 5 second period in response to light.

For food-deprivation experiments, flies were raised as above, except 48 hours before experiments, flies were wet-starved by placing them in a vial with a water saturated kimwipe supplemented with .4 mM retinal. Flies were activated with a 635 nm laser at four different light intensities: 1.8, 8.9, 17.8 and 153 uW/mm^2.

GtACR1 silencing

Three-day-old female flies were raised on standard food, and transferred to standard food with 0.4 mM all-trans retinal for two days. Next, flies were wet-starved with 0.4 mM retinal in water for 24 hours. Flies were anesthetized with carbon dioxide, mounted onto a glass slide with nail polish, and allowed to recover for two hours in a humidified chamber at 22°C. A green laser (532 nm, LaserGlow LBS-532) was used to acutely silence neurons using GtACR1 (Mohammad et al., 2017). Flies were water satiated,

then presented with either 50 mM sucrose or 100 mM sucrose three times to the proboscis, and the number of flies that extended at least once were recorded.

***In vivo* sample preparation for calcium Imaging**

Mated female flies were dissected for calcium imaging studies 14 to 21 days post-eclosion as previously described (Harris et al., 2015) with the following modifications. Flies were briefly anesthetized with ice as they were placed in a custom plastic holder at the cervix to isolate the head from the rest of the body. Then, the head was then immobilized using UV glue. To provide unobstructed imaging access to the SEZ, the esophagus was cut. Fed, starved, desiccated, and pseudodessicated (thirsty-like) conditions were accomplished as follows:

Fed: Flies were placed in a fresh vial containing standard cornmeal-yeast-molasses media 18-24 hours prior to imaging. Following dissection, samples were bathed in ~250 mOsmo Artificial Hemolymph-Like solution (AHL) ("artificial hemolymph") and imaged immediately.

Food-deprived: Flies were food deprived in a vial containing a wet kimwipe for 18-24 hours prior to imaging. Following dissection, samples were bathed in ~250 mOsmo AHL and imaged immediately.

Desiccated: Flies were placed in a vial containing 5 grams of Drierite™ for two hours. A cotton ball was used to isolate flies from the desiccant inside the vial, and the vial was closed with parafilm to create a dry chamber. Following dissection, samples were bathed in ~250 mOsmo AHL and imaged immediately. Hemolymph signals of thirst, such as osmolality, may be perturbed in our calcium imaging studies, limiting our ability to accurately assess a thirsty state (Jourjine et al., 2016).

Thirsty-like (Pseudodessicated): Flies were placed in a fresh vial containing standard cornmeal-yeast-molasses media 18-24 hours prior to imaging. Following dissection, samples were bathed in ~350 mOsmo AHL ("high osmolality artificial hemolymph") and allowed to rest for one hour prior to imaging.

Calcium imaging with taste stimulation

For imaging responses to taste solutions, females of UAS-CD8-tdTomato;20XUAS-IVS-GCaMP6s(attP5);20XUAS-IVS-GCaMP6s(VK00005) were crossed to males for each split-GAL4 line, and female progeny without balancers were selected for imaging. The following tastants were used: double-distilled water ("water"), 1M sucrose ("sugar"), or 10 mM denatonium plus 100 mM caffeine in 20% polyethylene glycol (PEG) ("bitter"). Taste solutions were delivered to the proboscis using a glass capillary (1.0 mm OD/ 0.78 mm ID) filled with ~4 μL of taste solution and positioned at the tip of the proboscis using a micromanipulator. Taste solutions were drawn away from the tip of the capillary at the beginning of each imaging trial using slight suction generated by an attached 1 mL syringe, and delivered to the proboscis at the relevant time during imaging with light pressure applied to the syringe.

Calcium imaging was performed using either a 1-photon or 2-photon microscope. For cell types in close proximity to the surface of the SEZ, 1-photon imaging was performed using a 3i spinning disc confocal microscope with a piezo drive and a 20x water immersion objective (NA=1.0) with a 2.5x magnification changer. 55 frames of 8 z sections spaced at 1 micron intervals were binned 4x4 and acquired at 0.8 Hz using a 488 nm laser. Taste solutions were in contact with the proboscis labellum from frame 20 to frame 25. Cell types imaged using a 1-photon microscope are Clavicle, Fdg, FMIn,

G2N-1, Phantom, Usnea, and Zorro. For cell types that arborize deeper in the SEZ, 2-photon imaging was performed using a Scientifica Hyperscope with resonant scanning, a piezo drive, and a 20x water immersion objective (NA=1.0) with 4x digital zoom. 80 stacks of 20 z sections spaced at 2 micron intervals were acquired at 0.667 Hz using a 920 nm laser. Taste solutions were in contact with the proboscis labellum from frame 30 to frame 40. Cell types imaged using a 2-photon microscope are Bract, Rattle, and Roundup.

Calcium imaging with optogenetic activation of gustatory receptor neurons

For imaging responses in the Fdg cell type to optogenetic activation of gustatory receptor neurons, females of 13XLexAop2-IVS-p10-ChrimsonR-mCherry(attP18);Gr5a-LexA;20XUAS-IVS-jGCaMP7b(VK00005), 13XLexAop2-IVS-p10-ChrimsonR-mCherry(attP18);20XUAS-IVS-jGCaMP7b(attP5); ppk28-LexA, or 13XLexAop2-IVS-p10-ChrimsonR-mCherry(attP18);20XUAS-IVS-jGCaMP7b(attP5); Gr66a-LexA were crossed to males of SS46913 (Sterne et al. 2021). For sugar and bitter integration experiments, virgins of a stock composed of either SS47082 (G2N-1) or SS47744 (Roundup) and 20xUAS-IVS-Syn21-Syt::Op-jGCaMP7b(attP18) were crossed to males of 13XLexAop2-IVS-p10-ChrimsonR-mCherry(attP18); Gr5a-LexA::VP16(12-1);, 13XLexAop2-IVS-p10-ChrimsonR-mCherry(attP18);Gr5a-LexA::VP16(12-1); Gr66a-LexA, or 13XLexAop2-IVS-p10-ChrimsonR-mCherry(attP18);;Gr66a-LexA; and female progeny without balancers were selected for imaging. 2-photon imaging was performed as described above for imaging with taste stimulation, but 660 nm light was used to activate gustatory receptor neurons in place of direct stimulation of the proboscis with taste solutions. Two-second light pulses were delivered three times at 10-second

intervals during imaging, and light was delivered through the objective in a widefield fashion under the control of a custom ScanImage plugin.

Calcium imaging analysis

Image analysis was carried out in Fiji (Schindelin et al., 2012), CircuitCatcher (Bushey 2021), Python, and R. First, in Fiji, Z stacks for each time point were maximum intensity projected and then movement corrected using the StackReg plugin with 'Rigid Body' or 'Translation' transformation (Thevenaz et al. 1998). Next, using CircuitCatcher, an ROI containing the neurites of the cell type of interest was selected along with a background ROI, and average fluorescence intensity for each ROI at each timepoint was retrieved. Then, in Python, background subtraction was carried out for each timepoint (F_t). To calculate $F_{initial}$, initial fluorescence intensity was calculated as the mean corrected average fluorescence intensity from frame 9 to 18 (for 1-photon imaging) or frame 0 to 19 (for 2-photon imaging and optogenetic imaging). Finally, the following formula was used to calculate ΔF/F: F_t-$F_{initial}$/$F_{initial}$. Area under the curve was approximated with the trapezoidal rule in Python using the NumPy.trapz function. Area under the curve was assessed from frames 20 to 25 (for 1-photon imaging), from frames 30 to 40 (for 2-photon imaging with taste stimulation), from frames 15 to 18 (for 2-photon imaging with optogenetic activation).

QUANTIFICATION AND STATISTICAL ANALYSIS

Statistical tests for behavioral assays were performed in Prism. For analysis of Proboscis Extension Response Assays, Fisher's Exact Test was used in comparing the fraction of PER responses in experimental versus control flies. Statistical analysis of

calcium imaging was carried out in R and Python. For imaging experiments carried out in a block design with three treatments (Figure 4, Figure S4), Quade tests were carried out in R using the PMCMRplus package (Thorsten 2021). Quade test was chosen because it is more powerful than Friedman for a block-design experiment with three treatments (Conovoer, 1999). Other statistical analyses of calcium imaging were carried out in Python using the SciPy (Virtanen et al. 2020) and scikit-posthocs packages (Therpilowski 2019).

Figure S1

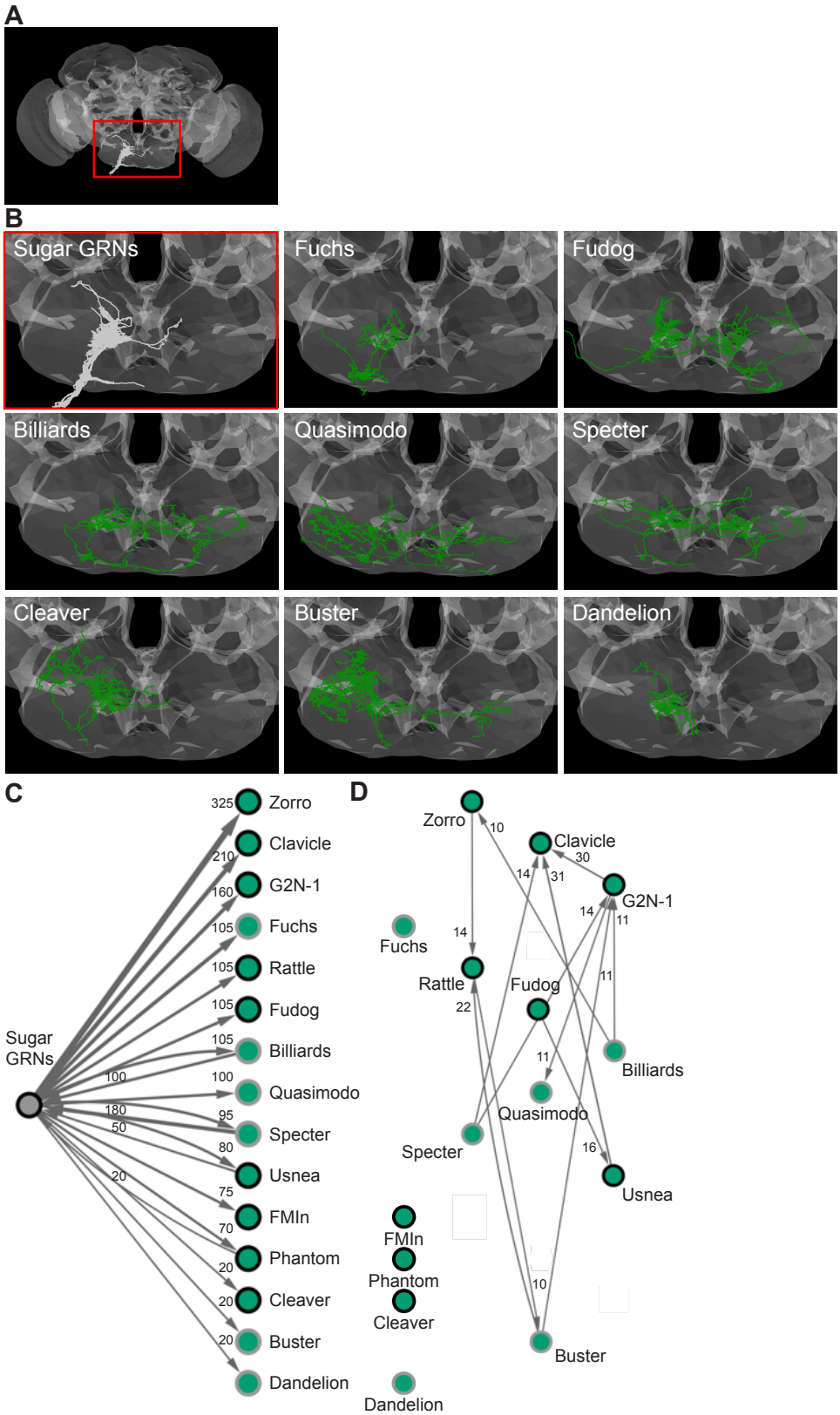
A
B
Sugar GRNs
Fuchs
Fudog
Billiards
Quasimodo
Specter
Cleaver
Buster
Dandelion
C
Sugar GRNs
325
Zorro
210
Clavicle
160
G2N-1
105
Fuchs
105
Rattle
105
Fudog
105
Billiards
100
Quasimodo
95
Specter
80
Usnea
75
FMIn
70
Phantom
20
Cleaver
20
Buster
20
Dandelion
100
180
50
20
D
Zorro
10
Clavicle
30
14
31
G2N-1
14
11
Fuchs
14
Rattle
22
Fudog
11
11
Billiards
Quasimodo
Specter
16
Usnea
FMIn
Phantom
Cleaver
10
Buster
Dandelion

Figure S1. Anatomy of reconstructed second-order neurons and their connectivity, Related to Figure 1. (A) Schematic of the entire fly brain, showing EM reconstructed sugar-sensing gustatory receptor neurons (GRNs) in gray. Area outlined in red is enlarged in the first panel of (B). (B) Anatomy of second-order candidate sugar EM reconstructed neurons. (C) Synaptic connectivity from sugar GRNs onto and from second-order neurons. Second-order neurons identified by EM and present in a split-Gal4 line (black circles); second-order neurons identified by EM only (grey circles). (D) Synaptic connectivity between second-order sugar neurons.

Figure S2

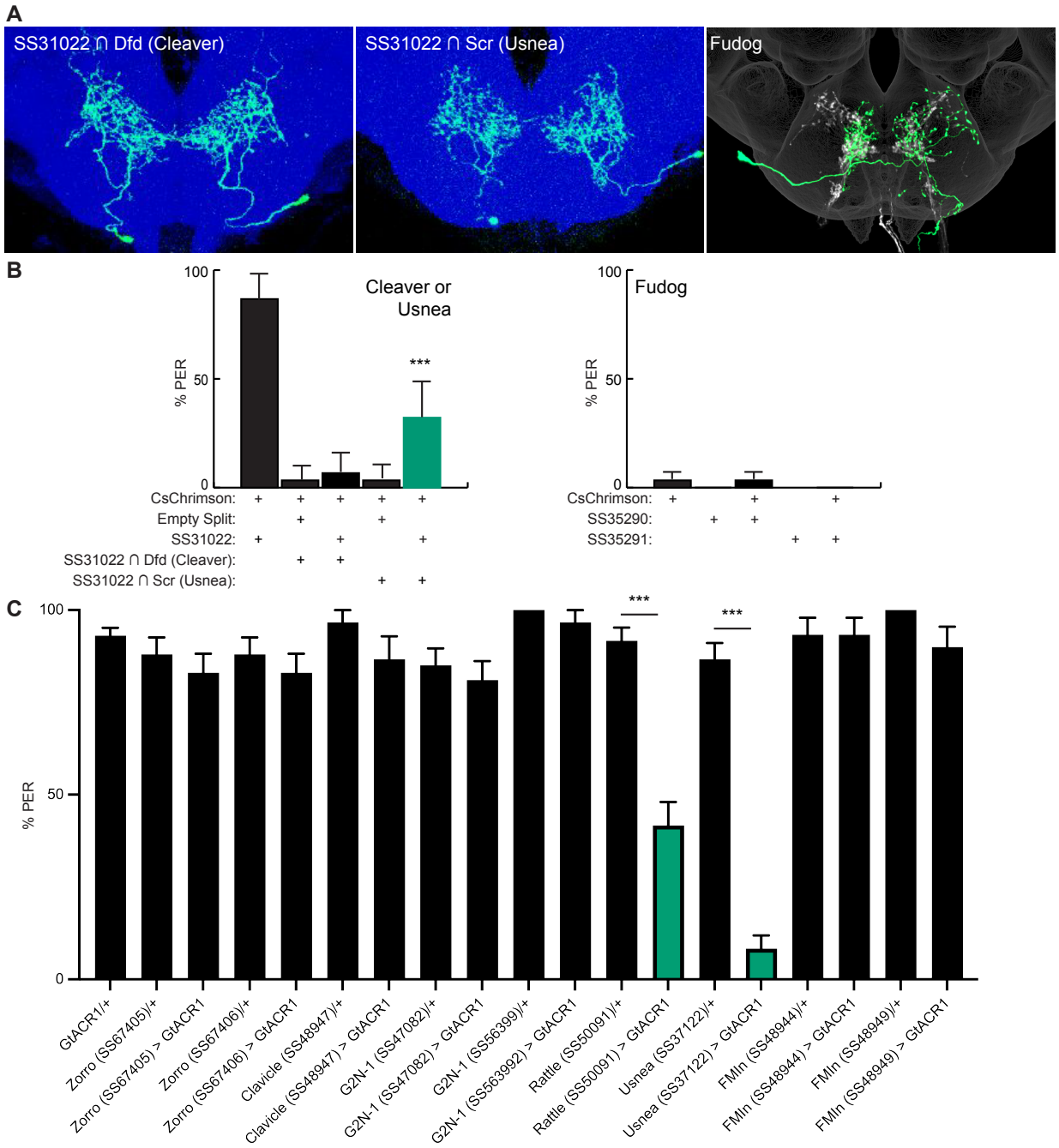

Figure S2. Additional proboscis extension phenotypes of second order neurons, Related to Figure 2. (A) Light microscopy images of Cleaver, Usnea and Fudog.

Cleaver and Usnea specific lines were generated using a triple-intersection approach (see Methods). In the Fudog image, sugar GRNs are depicted in white. (B) Activation of Usnea, but not Cleaver or Fudog, elicits proboscis extension. (C) Hyperpolarization of Rattle and Usnea inhibited proboscis extension to 100 mM sucrose, but hyperpolarization of other second-order neurons did not.

Figure S3

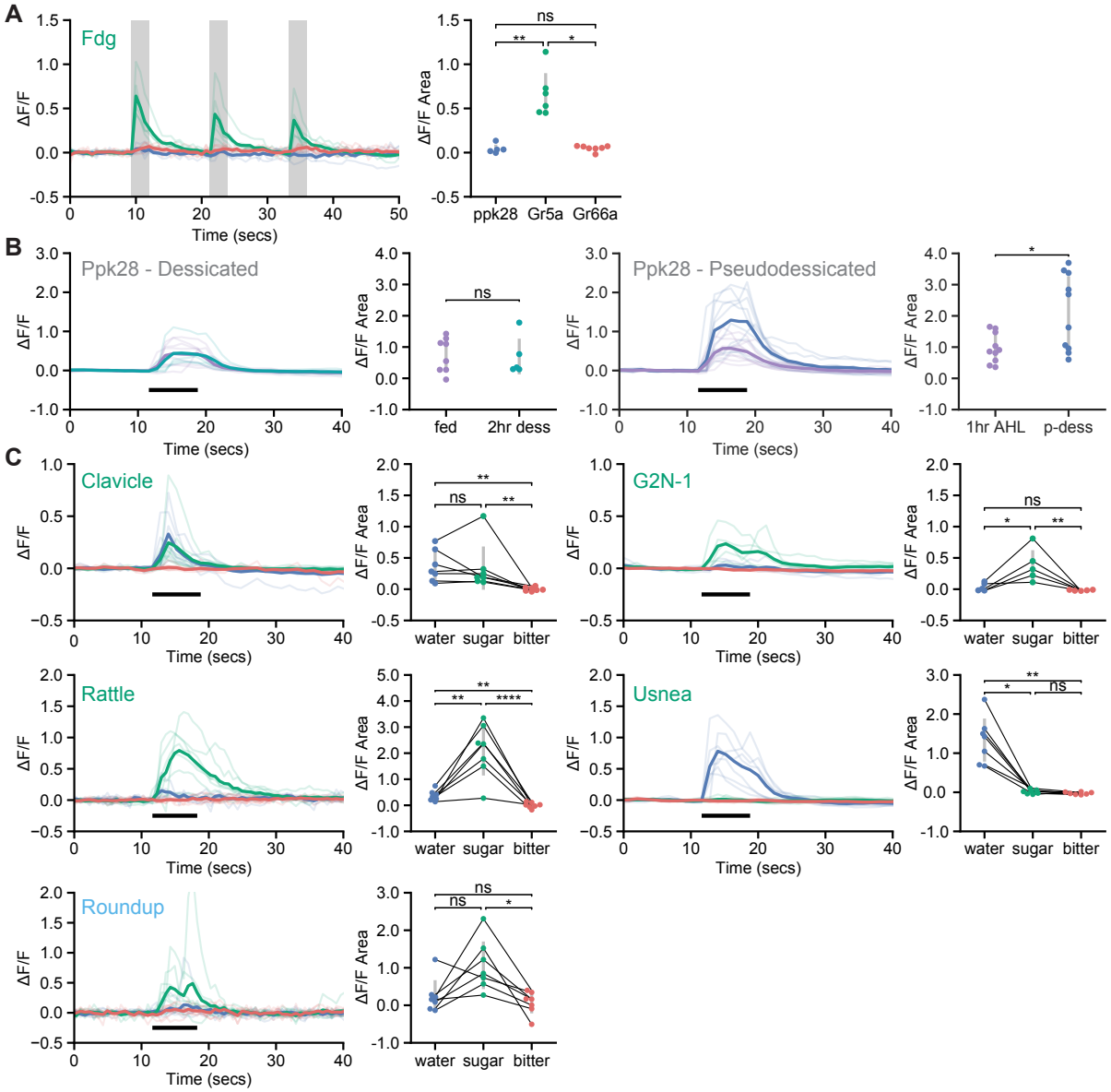

Figure S3. Taste responses of feeding initiation neurons, Related to Figure 4.

(A) Calcium responses of Fdg to optogenetic activation of water (blue, ppk28-LexA), sugar (green, Gr5a-LexA), or bitter (red, Gr66a-LexA) GRNs in starved flies. To examine Fdg responses, GCaMP7b was expressed using SS46913. Fluorescence traces are shown on the left of the panel (ΔF/F), while ΔF/F area for each trace is

shown on the right. Stimulation with 660 nm light is indicated with vertical grey bars. Kruskal Wallace test with Dunn's test using Holm's correction to adjust for multiple comparisons, ns $p>0.05$, *$p\leq0.05$, **$p\leq0.01$. (B-C) Calcium responses of water gustatory sensory neurons and feeding initiation neurons to taste stimulation of the proboscis. GCaMP6s fluorescence traces are shown on the left of each panel ($\Delta F/F$), while $\Delta F/F$ area for each trace is shown on the right. Significance levels: ns $p>0.05$, *$p\leq0.05$, **$p\leq0.01$, ***$p\leq0.001$, ***$p\leq0.0001$. (B) Taste responses to water in fed (purple) versus two hour desiccated (2hr dess, teal) flies (left). Taste responses to water in fed flies allowed to rest for one hour in low osmolality artificial hemolymph after dissection before imaging (1hr fed, purple) versus pseudodessicated, thirsty-like flies (p-dess, blue) (right). (C) Taste responses in pseudodessicated, thirsty-like flies. The proboscis of each tested individual was stimulated with water (green), sugar (blue), and bitter (red) tastants in sequential trials during the indicated period (thick black line). Thin black lines indicate sample pairing. The following split-GAL4 lines were imaged for each cell type: Clavicle; SS48947, G2N-1; SS47082, Usnea; SS37122, Rattle; SS50091, Roundup; SS47744. Quade's Test with Quade's All Pairs Test, using Holm's correction to adjust for multiple comparisons.

Table S1

Table S1-A This table indicates the number of synapses between sugar GRNs and second-order sugar neurons, from manually annotated CATMAID skeletons

	G2N-1	Phantom	GRN 7349220	GRN 7349286	GRN 7432035	GRN 7456678	GRN 7468836	GRN 7471729	GRN 7487872	GRN 7708436	GRN 7723219	GRN 7724245	GRN 7753062	GRN 7774115	GRN 7793753	GRN 10742201	GRN 11206722	GRN 4644404161	GRN 4903508810	Rattle	Billiards	Zorro	Fuchs	Fudog	Quasimodo	FMIn	Clavicle	Usnea	Fdg	Specter
G2N-1	0	0	0	0	0	0	0	0	0	0	0	0	0	0	0	0	0	0	0	5	1	0	3	0	11	7	30	0	4	0
Phantom	0	0	0	3	0	0	0	0	2	0	5	5	0	0	0	0	1	5	0	0	0	0	0	0	0	0	0	0	0	0
GRN 7349220	18	2	0	3	2	18	1	0	8	24	1	0	1	11	8	11	4	2	17	11	8	25	29	7	9	9	16	5	0	3
Sugar GRN 7349286	7	8	4	1	2	2	1	0	9	4	7	14	0	2	3	2	0	22	0	1	1	21	4	15	8	0	12	4	0	1
Sugar GRN 7432035	10	3	3	4	0	3	0	1	10	1	0	2	1	4	10	21	2	4	13	13	15	35	3	6	9	4	27	2	0	10
Sugar GRN 7456678	4	0	29	1	2	0	1	8	4	8	0	0	4	18	16	2	5	3	14	14	3	28	15	1	3	1	4	3	0	0
Sugar GRN 7468836	4	10	0	1	1	0	0	31	0	0	1	2	31	4	0	0	26	0	2	0	1	1	6	1	3	1	2	10	0	7
Sugar GRN 7471729	2	4	1	0	0	4	17	1	0	0	0	0	23	6	1	1	24	0	1	2	6	4	16	0	3	1	2	1	0	3
Sugar GRN 7487872	38	6	9	5	9	1	0	1	0	5	0	2	1	4	4	16	0	6	7	6	17	36	4	1	14	13	40	4	1	8
Sugar GRN 7708436	3	0	14	1	0	4	1	1	3	1	1	0	0	7	11	3	2	2	8	8	2	14	13	3	8	4	11	3	0	3
Sugar GRN 7723219	7	0	4	6	5	1	0	1	4	0	0	17	0	0	0	11	2	8	1	0	3	10	7	6	1	0	7	1	0	0
Sugar GRN 7724245	3	4	4	7	3	0	1	0	5	0	7	0	1	1	0	9	0	7	0	1	0	12	3	21	4	0	4	5	0	3
Sugar GRN 7753062	2	8	5	0	1	3	33	19	2	0	0	0	0	11	5	0	29	0	6	0	6	7	11	4	4	5	0	10	0	7
Sugar GRN 7774115	6	4	13	1	3	25	3	6	4	14	1	1	12	0	10	2	19	3	18	14	4	25	28	4	11	0	4	1	0	11
Sugar GRN 7793753	7	1	9	4	4	10	0	1	6	18	0	2	3	10	0	4	3	6	25	9	8	23	9	3	7	3	15	3	0	6
Sugar GRN 10742201	44	6	13	1	14	4	0	0	12	2	2	6	0	2	4	0	2	2	3	1	20	34	5	6	9	26	46	7	1	21
Sugar GRN 11206722	2	5	4	1	2	5	14	28	0	2	2	0	24	14	3	0	0	0	9	6	7	10	5	3	2	2	1	12	0	7
Sugar GRN 4644404161	3	6	9	16	5	0	0	0	5	0	11	9	1	2	1	6	0	0	2	3	1	23	7	10	3	1	9	3	0	2
Sugar GRN 4903508810	3	0	10	3	5	10	0	2	7	9	0	0	3	10	15	3	3	2	0	18	7	18	13	3	0	4	11	2	2	6
Rattle	0	0	0	0	0	0	0	0	0	0	0	0	0	0	0	0	0	0	0	0	0	4	0	0	3	0	3	0	11	1
Billiards	11	1	4	0	9	4	0	0	21	8	0	0	1	7	5	36	0	0	5	1	1	10	0	1	0	2	9	1	0	1
Zorro	0	0	0	0	0	0	0	0	1	0	0	0	0	0	0	0	0	0	0	14	0	0	0	0	3	8	1	0	2	0
Fuchs	0	0	0	0	0	0	0	0	0	0	0	0	0	0	0	0	0	0	0	0	1	0	0	0	0	0	0	0	0	0
Fudog	0	2	1	0	0	0	0	0	1	0	0	0	0	0	0	1	0	0	0	0	0	3	0	0	1	7	0	16	1	1
Quasimodo	0	0	0	0	0	0	0	0	0	0	0	0	0	0	0	0	0	0	0	0	0	0	0	0	1	0	0	0	0	0
FMIn	1	0	0	0	0	0	0	0	0	0	0	0	0	0	0	0	0	0	0	2	0	1	1	0	0	0	0	0	6	0
Clavicle	2	1	0	0	1	0	0	0	2	0	0	0	0	0	2	2	0	0	0	0	0	0	0	0	0	2	1	5	1	3
Usnea	6	0	5	2	2	1	3	2	4	1	1	1	3	3	1	3	3	0	3	0	0	3	1	3	0	0	31	0	0	1
Fdg	0	1	0	0	0	0	0	0	0	0	0	0	0	0	0	0	0	0	0	1	0	1	0	0	13	19	0	0	1	0
Specter	14	1	15	0	29	4	3	0	29	8	0	0	0	9	16	47	3	0	14	4	0	5	0	2	1	4	14	1	0	0

Table S1. Synaptic connectivity between feeding initiation neurons; Flywire predictions of synaptic connectivity, Related to Figure 1. (A) Connectivity between sugar GRNs and second-order sugar neurons. (B) Connectivity between all neurons identified in this paper. (C) CATMAID Skeleton names and IDs. (D) Second-order sugar neurons and connectivity as identified in the Flywire annotation platform. (E) Third-order sugar neurons and connectivity from Flywire. (F) MN9 premotor neurons and connectivity identified from Flywire. (G) Second-order bitter neurons and connectivity identified from Flywire.

REFERENCES

Augustine, V., Gokce, S.K., and Oka, Y. (2018). Peripheral and Central Nutrient Sensing Underlying Appetite Regulation. Trends in Neurosciences *41*, 526–539.

Bates, A.S., Schlegel, P., Roberts, R.J.V., Drummond, N., Tamimi, I.F.M., Turnbull, R., Zhao, X., Marin, E.C., Popovici, P.D., Dhawan, S., et al. (2020a). Complete Connectomic Reconstruction of Olfactory Projection Neurons in the Fly Brain. Current Biology *30*, 3183-3199.e6.

Bates, A.S., Manton, J.D., Jagannathan, S.R., Costa, M., Schlegel, P., Rohlfing, T., and Jefferis, G.S. (2020b). The natverse, a versatile toolbox for combining and analysing neuroanatomical data. ELife *9*, e53350.

Buhmann, J., Sheridan, A., Malin-Mayor, C., Schlegel, P., Gerhard, S., Kazimiers, T., Krause, R., Nguyen, T.M., Heinrich, L., Lee, W.-C.A., et al. (2021). Automatic detection of synaptic partners in a whole-brain Drosophila electron microscopy data set. Nat Methods *18*, 771–774.

Chalasani, S.H., Kato, S., Albrecht, D.R., Nakagawa, T., Abbott, L.F., and Bargmann, C.I. (2010). Neuropeptide feedback modifies odor-evoked dynamics in *Caenorhabditis elegans* olfactory neurons. Nat Neurosci *13*, 615–621.

Chao, M.Y., Komatsu, H., Fukuto, H.S., Dionne, H.M., and Hart, A.C. (2004). Feeding status and serotonin rapidly and reversibly modulate a *Caenorhabditis elegans* chemosensory circuit. Proceedings of the National Academy of Sciences *101*, 15512–15517.

Chen, T., Wardill, T. Sun, Y., Pulver, S., Renninger, S., Baohan, A., Schreiter, E., Kerr, R., Orger, M., Jayaraman, V., et al. (2013). Ultrasensitive fluorescent proteins for imaging neuronal activity. Nature *499*, 295-300.

Chiu, H., Hoopfer, E.D., Coughlan, M.L., Pavlou, H.J., Goodwin, S.F., and Anderson, D.J. (2021). A circuit logic for sexually shared and dimorphic aggressive behaviors in *Drosophila*. Cell *184*, 507-520.e16.

Chu, B., Chui, V., Mann, K., and Gordon, M.D. (2014). Presynaptic Gain Control Drives Sweet and Bitter Taste Integration in *Drosophila*. Current Biology *24*, 1978–1984.

Conover, W.J. (1999). Practical nonparametric statistics (New York: Wiley).

Costa, M., Manton, J.D., Ostrovsky, A.D., Prohaska, S., and Jefferis, G.S.X.E. (2016). NBLAST: Rapid, Sensitive Comparison of Neuronal Structure and Construction of Neuron Family Databases. Neuron *91*, 293–311.

Dethier, V.G. (1976). The hungry fly: a physiological study of the behavior associated with feeding (Cambridge, Mass: Harvard University Press).

Dorkenwald, S., McKellar, C.E., Macrina, T., Kemnitz, N., Lee, K., Lu, R., Wu, J., Popovych, S., Mitchell, E., Nehoran, B., et al. (2022). FlyWire: online community for whole-brain connectomics. Nat Methods *19*, 119–128.

Flood, T.F., Iguchi, S., Gorczyca, M., White, B., Ito, K., and Yoshihara, M. (2013). A single pair of interneurons commands the *Drosophila* feeding motor program. Nature *499*, 83–87.

French, A.S., Sellier, M.-J., Ali Agha, M., Guigue, A., Chabaud, M.-A., Reeb, P.D., Mitra, A., Grau, Y., Soustelle, L., and Marion-Poll, F. (2015). Dual Mechanism for Bitter Avoidance in *Drosophila*. Journal of Neuroscience *35*, 3990–4004.

Gordon, M.D., and Scott, K. (2009). Motor Control in a *Drosophila* Taste Circuit. Neuron *61*, 373–384.

Gray, J.M., Hill, J.J., and Bargmann, C.I. (2005). A circuit for navigation in *Caenorhabditis elegans*. Proc. Natl. Acad. Sci. U.S.A. *102*, 3184–3191.

Harris, D.T., Kallman, B.R., Mullaney, B.C., and Scott, K. (2015). Representations of Taste Modality in the *Drosophila* Brain. Neuron *86*, 1449–1460.

Hartenstein, V., Omoto, J.J., Ngo, K.T., Wong, D., Kuert, P.A., Reichert, H., Lovick, J.K., and Younossi-Hartenstein, A. (2018). Structure and development of the subesophageal zone of the *Drosophila* brain. I. Segmental architecture, compartmentalization, and lineage anatomy. J Comp Neurol *526*, 6–32.

Heinrich, L., Funke, J., Pape, C., Nunez-Iglesias, J., and Saalfeld, S. (2018). Synaptic Cleft Segmentation in Non-Isotropic Volume Electron Microscopy of the Complete *Drosophila* Brain. ArXiv:1805.02718 [Cs].

Inagaki, H.K., Ben-Tabou de-Leon, S., Wong, A.M., Jagadish, S., Ishimoto, H., Barnea, G., Kitamoto, T., Axel, R., and Anderson, D.J. (2012). Visualizing Neuromodulation In Vivo: TANGO-Mapping of Dopamine Signaling Reveals Appetite Control of Sugar Sensing. Cell *148*, 583–595.

Inagaki, H.K., Panse, K.M., and Anderson, D.J. (2014). Independent, Reciprocal Neuromodulatory Control of Sweet and Bitter Taste Sensitivity during Starvation in *Drosophila*. Neuron *84*, 806–820.

Jeong, Y.T., Shim, J., Oh, S.R., Yoon, H.I., Kim, C.H., Moon, S.J., and Montell, C. (2013). An Odorant-Binding Protein Required for Suppression of Sweet Taste by Bitter Chemicals. Neuron *79*, 725–737.

Jin, H., Fishman, Z.H., Ye, M., Wang, L., and Zuker, C.S. (2021). Top-Down Control of Sweet and Bitter Taste in the Mammalian Brain. Cell *184*, 257-271.e16.

Jourjine, N., Mullaney, B.C., Mann, K., and Scott, K. (2016). Coupled Sensing of Hunger and Thirst Signals Balances Sugar and Water Consumption. Cell *166*, 855–866.

Kain, P., and Dahanukar, A. (2015). Secondary Taste Neurons that Convey Sweet Taste and Starvation in the *Drosophila* Brain. Neuron *85*, 819–832.

Kawai, K., Sugimoto, K., Nakashima, K., Miura, H., and Ninomiya, Y. (2000). Leptin as a modulator of sweet taste sensitivities in mice. Proc. Natl. Acad. Sci. U.S.A. *97*, 11044–11049.

Kendroud, S., Bohra, A.A., Kuert, P.A., Nguyen, B., Guillermin, O., Sprecher, S.G., Reichert, H., VijayRaghavan, K., and Hartenstein, V. (2018). Structure and development of the subesophageal zone of the *Drosophila* brain. II. Sensory compartments. J Comp Neurol *526*, 33–58.

Klapoetke, N.C., Murata, Y., Kim, S.S., Pulver, S.R., Birdsey-Benson, A., Cho, Y.K., Morimoto, T.K., Chuong, A.S., Carpenter, E.J., Tian, Z., et al. (2014). Independent optical excitation of distinct neural populations. Nat Methods *11*, 338–346.

LeDue, E.E., Mann, K., Koch, E., Chu, B., Dakin, R., and Gordon, M.D. (2016). Starvation-Induced Depotentiation of Bitter Taste in *Drosophila*. Current Biology *26*, 2854–2861.

Leopold, P., and Perrimon, N. (2007). *Drosophila* and the genetics of the internal milieu. Nature *450*, 186–188.

Li, P.H., Lindsey, L.F., Januszewski, M., Zheng, Z., Bates, A.S., Taisz, I., Tyka, M., Nichols, M., Li, F., Perlman, E., et al. (2019). Automated Reconstruction of a Serial-Section EM *Drosophila* Brain with Flood-Filling Networks and Local Realignment (Neuroscience).

Liman, E., Zhang, Y., and Montell, C. (2014). Peripheral Coding of Taste. Neuron *81*, 984–1000.

Mann, K., Gordon, M.D., and Scott, K. (2013). A Pair of Interneurons Influences the Choice between Feeding and Locomotion in *Drosophila*. Neuron *79*, 754–765.

Marella, S., Mann, K., and Scott, K. (2012). Dopaminergic Modulation of Sucrose Acceptance Behavior in *Drosophila*. Neuron *73*, 941–950.

McKellar, C.E., Siwanowicz, I., Dickson, B.J., and Simpson, J.H. (2020). Controlling motor neurons of every muscle for fly proboscis reaching. ELife *9*, e54978.

Meunier, N., Marion-Poll, F., Rospars, J.-P., and Tanimura, T. (2003). Peripheral coding of bitter taste in *Drosophila*. J. Neurobiol. *56*, 139–152.

Miyazaki, T., and Ito, K. (2010). Neural architecture of the primary gustatory center of *Drosophila melanogaster* visualized with GAL4 and LexA enhancer-trap systems. J. Comp. Neurol. *518*, 4147–4181.

Miyazaki, T., Lin, T.-Y., Ito, K., Lee, C.-H., and Stopfer, M. (2015). A gustatory second-order neuron that connects sucrose-sensitive primary neurons and a distinct region of the gnathal ganglion in the *Drosophila* brain. Journal of Neurogenetics *29*, 144–155.

Mohammad, F., Stewart, J.C., Ott, S., Chlebikova, K., Chua, J.Y., Koh, T.-W., Ho, J., and Claridge-Chang, A. (2017). Optogenetic inhibition of behavior with anion channelrhodopsins. Nat Methods *14*, 271–274.

Montell, C. (2021). *Drosophila* sensory receptors—a set of molecular Swiss Army Knives. Genetics *217*, 1–34.

Nässel, D.R., and Zandawala, M. (2019). Recent advances in neuropeptide signaling in *Drosophila*, from genes to physiology and behavior. Progress in Neurobiology *179*, 101607.

Peng, Y., Gillis-Smith, S., Jin, H., Tränkner, D., Ryba, N.J.P., and Zuker, C.S. (2015). Sweet and bitter taste in the brain of awake behaving animals. Nature *527*, 512–515.

Pool, A.-H., and Scott, K. (2014). Feeding regulation in *Drosophila*. Current Opinion in Neurobiology *29*, 57–63.

Root, C.M., Ko, K.I., Jafari, A., and Wang, J.W. (2011). Presynaptic Facilitation by Neuropeptide Signaling Mediates Odor-Driven Food Search. Cell *145*, 133–144.

Saalfeld, S., Cardona, A., Hartenstein, V., and Tomancak, P. (2009). CATMAID: collaborative annotation toolkit for massive amounts of image data. Bioinformatics *25*, 1984–1986.

Savigner, A., Duchamp-Viret, P., Grosmaitre, X., Chaput, M., Garcia, S., Ma, M., and Palouzier-Paulignan, B. (2009). Modulation of Spontaneous and Odorant-Evoked Activity of Rat Olfactory Sensory Neurons by Two Anorectic Peptides, Insulin and Leptin. Journal of Neurophysiology *101*, 2898–2906.

Schindelin, J., Arganda-Carreras, I., Frise, E., Kaynig, V., Longair, M., Pietzsch, T., Preibisch, S., Rueden, C., Saalfeld, S., Schmid, B., et al. (2012). Fiji: an open-source platform for biological-image analysis. Nat Methods *9*, 676–682.

Schlegel, P., Bates, A.S., Stürner, T., Jagannathan, S.R., Drummond, N., Hsu, J., Serratosa Capdevila, L., Javier, A., Marin, E.C., Barth-Maron, A., et al. (2021). Information flow, cell types and stereotypy in a full olfactory connectome. ELife *10*, e66018.

Schwarz, O., Bohra, A.A., Liu, X., Reichert, H., VijayRaghavan, K., and Pielage, J. (2017). Motor control of *Drosophila* feeding behavior. ELife *6*, e19892.

Scott, K. (2018). Gustatory Processing in *Drosophila melanogaster*. Annu. Rev. Entomol. *63*, 15–30.

Sengupta, P. (2013). The belly rules the nose: feeding state-dependent modulation of peripheral chemosensory responses. Current Opinion in Neurobiology *23*, 68–75.

Sterne, G.R., Otsuna, H., Dickson, B.J., and Scott, K. (2021). Classification and genetic targeting of cell types in the primary taste and premotor center of the adult Drosophila brain. ELife *10*, e71679.

Stocker, R.F., and Schorderet, M. (1981). Cobalt filling of sensory projections from internal and external mouthparts in *Drosophila*. Cell Tissue Res. *216*.

Talay, M., Richman, E.B., Snell, N.J., Hartmann, G.G., Fisher, J.D., Sorkaç, A., Santoyo, J.F., Chou-Freed, C., Nair, N., Johnson, M., et al. (2017). Transsynaptic Mapping of Second-Order Taste Neurons in Flies by trans-Tango. Neuron *96*, 783-795.e4.

Terpilowski, M. (2019). scikit-posthocs: Pairwise multiple comparison tests in Python. JOSS *4*, 1169.

Virtanen, P., Gommers, R., Oliphant, T.E., Haberland, M., Reddy, T., Cournapeau, D., Burovski, E., Peterson, P., Weckesser, W., Bright, J., et al. (2020). SciPy 1.0: fundamental algorithms for scientific computing in Python. Nat Methods *17*, 261–272.

Wang, L., Gillis-Smith, S., Peng, Y., Zhang, J., Chen, X., Salzman, C.D., Ryba, N.J.P., and Zuker, C.S. (2018). The coding of valence and identity in the mammalian taste system. Nature *558*, 127–131.

Yarmolinsky, D.A., Zuker, C.S., and Ryba, N.J.P. (2009). Common Sense about Taste: From Mammals to Insects. Cell *139*, 234–244.

Zheng, Z., Lauritzen, J.S., Perlman, E., Robinson, C.G., Nichols, M., Milkie, D., Torrens, O., Price, J., Fisher, C.B., Sharifi, N., et al. (2018). A Complete Electron Microscopy Volume of the Brain of Adult *Drosophila melanogaster*. Cell *174*, 730-743.e22.